



ELSEVIER

doi:10.1016/j.gca.2004.06.005

Surface charge evolution of mineral-organic complexes during pedogenesis in Hawaiian basalt

JON CHOROVER,^{1,*} MARY KAY AMISTADI,¹ and OLIVER A. CHADWICK²¹Department of Soil, Water and Environmental Science, University of Arizona, Tucson, Arizona 85721-0038 USA²Department of Geography, University of California, Santa Barbara, Santa Barbara, California 93106 USA

(Received December 16, 2003; accepted in revised form June 14, 2004)

Abstract—Changes in surface charge of soil particles that accompany mineral transformations during soil formation were measured for a humid tropical chronosequence in Hawaiian basalt ranging in lava flow age from 0.3 to 4100 kiloyears (ky). Parent mineralogy is dominated by glass, olivine, pyroxene, and feldspar, whereas poorly crystalline (PC) weathering products (allophane, microcrystalline gibbsite, ferrihydrite) accumulate in early to intermediate weathering stages (through 400 ky), and crystalline secondary minerals (kaolinite, gibbsite, goethite) are dominant in the oldest (1400 and 4100 ky) soils. Detailed characterization of the solid phase was accomplished with chemical extractions, X-ray diffraction analysis, and molecular spectroscopy (FTIR and ¹³C MAS NMR). Simultaneous proton titration and background ion adsorption measurements were made on LiCl saturated soils over a range in pH (2–9) and ionic strength (0.001 and 0.01 M LiCl). Dependence of variable surface charge on solution composition reflects the changing nature of mineral-organic interactions over the course of pedogenesis. Points of zero net proton charge (PZNPC) ranged from 3.4 to 6.2 and 2.0 to 5.8 at 0.001 and 0.01 M ionic strength (*I*), respectively. Intermediate-aged soils containing the highest mass concentration of humified soil organic matter (SOM) and its complexes with PC minerals gave rise to the steepest charging curves (largest pH dependence) and highest PZNPC values. Surface charge properties of these soils most closely reflected their weakly acidic Al and Fe hydroxide constituents, which is consistent with metal hydroxide saturation of organic functional groups, rather than organic coating of mineral surfaces. Charging curves were less steep and PZNPC values were lower for the older soils, consistent with SOM coating of more crystalline goethite, kaolinite, and gibbsite surfaces in a soil system less impacted by labile Al and Fe. Copyright © 2004 Elsevier Ltd

1. INTRODUCTION

Soils derived from volcanic lava and tephra cover ca. 1% of the earth's land surface and give rise to a wide range of soil types, depending upon genetic drivers (climate, biota, topography, and time). The primary mineralogy of basalt (plagioclase feldspar, olivine, pyroxenes, and ferromagnetic minerals) weathers rapidly under high throughputs of water, owing to high mass concentrations of volcanic glass, chain and nesosilicates, and small crystallite sizes relative to other igneous rock (Lowe, 1986; Gislason and Arnórsson, 1993; Gislason et al., 1996). Ejecta from Hawaiian volcanoes comprises a mixture of lava and tephra. In the presence of sufficient fresh water, incipient weathering of Hawaiian volcanic ash and lava promotes rapid dissolution of Si, Al, Fe, and nonhydrolyzing cations (e.g., Ca, Mg) in "early" weathering stages. Whereas large quantities of the latter are removed via leaching, the former are retained preferentially due to precipitation of poorly crystalline (PC) solid phases (e.g., microcrystalline gibbsite, allophane, imogolite, and ferrihydrite) from supersaturated solutions. Prevalence of these metastable solids, which is characteristic of "intermediate" weathering stages in humid tropical soils derived from volcanic ejecta (Shoji et al., 1993; Chadwick et al., 2003), may be accompanied by a smaller accumulation of structurally charged 2:1 layer-type silicates (Chorover et al., 1999a). With continued throughput of water, soil mineralogy is

transformed to crystalline (C) minerals typical of "late" stage weathering, including halloysite or kaolinite, gibbsite, goethite, and hematite (Chadwick and Chorover, 2001).

Mineral evolution during pedogenesis should be accompanied by measurable changes in the surface chemistry of soil particles, which affects an array of biogeochemical processes including adsorption of nutrient or toxic ions, mineral weathering reactions, particle aggregation, and organic matter retention. PC secondary solids that are formed at intermediate weathering stages are known to have high specific surface area and reactive surface hydroxyl groups that should contribute significant variable charge per unit mass of bulk soil. Further, since leaching of soils by fresh water removes solid phase Si in preference to Al, Fe, and Ti (Sposito, 1989), the surface charge of soil mineral particles is expected to increase as the more strongly acidic silanol ($\equiv\text{SiOH}$) sites associated with primary minerals and metastable silicates are depleted relative to weakly acidic surface hydroxyl groups of Fe, Al, and Ti (hydr)oxides ($\equiv\text{FeOH}$, $\equiv\text{AlOH}$ and $\equiv\text{TiOH}$).

Volcanic ejecta is weathered rapidly in humid tropical climates, and soils support high biomass forest ecosystems relatively soon after deposition (<300 yr at 2.5 m mean annual precipitation [MAP] and 289 K [16°C]). A significant fraction of fixed carbon (biomolecules and humic substances) is input to the soil solution as dissolved organic matter (DOM) or is incorporated into the soil solid phase (Neff et al., 2000). In forests, soil organic matter (SOM) is critically important to soil particle charge, since it contains a diverse mixture of molecules and associated functional groups varying in acidity (Perdue and

* Author to whom correspondence should be addressed (chorover@cals.arizona.edu).

Table 1. Hawaiian long substrate age gradient (LSAG): Site descriptions and selected soil chemical data.

Soil sample	Age ¹ (ky)	Island location	Soil pH ³ (DI H ₂ O)	Org-C ⁴ (g kg ⁻¹)	Mineralogy ⁵	Structural charge ($-\sigma_0$) (mmol _c kg ⁻¹) ⁶
Surface						
(10–20 cm)						
Ola'a A	0.3 ³	Hawaii Volcanoes National Park, Hawaii	6.04 (0.04)	96 (9.5)	P, F, a	32 (0.55)
Laupahoehoe A	20	Laupahoehoe Forest Reserve, Hawaii	3.59 (0.02)	339 (4.5)	F, A, m, q	46 (3.97)
Kohala A	150	Kohala Forest Reserve, Hawaii	3.98 (0.06)	390 (14.0)	A, F, v, hiv, q	60 (4.63)
Pololu A	400	Koala Forest Reserve, Hawaii	3.70 (0.03)	136 (5.9)	A, F, v, hiv, k, q	91 (5.14)
Kolekole A	1400	Komakou Preserve, Molokai	3.82 (0.06)	125 (1.8)	K, Gi, F, he, q	26 (0.37)
Kokee A	4100	Napali-Kona Forest Reserve, Kauai	3.80 (0.06)	51 (1.4)	K, Gi, Go, he	15 (2.70)
Subsurface						
(50–70 cm)						
Ola'a B	0.3	—	6.60 (0.08)	6.3 (0.8)	P, F, a	36 (2.13)
Laupahoehoe B	20	—	4.69 (0.01)	116 (15.0)	F, A, m, q	16 (0.59)
Kohala B	150	—	4.23 (0.02)	32 (4.2)	A, F, hiv, q	69 (3.44)
Pololu B	400	—	4.03 (0.06)	104 (6.5)	A, F, v, hiv, k, q	27 (0.70)
Kolekole B	1400	—	4.27 (0.04)	19 (7.2)	K, Gi, f, he, q, m	29 (4.10)
Kokee B	4100	—	4.11 (0.02)	14 (3.6)	K, Gi, Go, he, m	3.0 (0.32)

¹ Parent material age, which is given in thousands of years (ky), was dated using K/Ar radiometric techniques.

² Ola'a soil is developed in Keanakakoi ash (deposited 200–300 ya) that overlies soil derived from Uwekahuna ash (deposited 2.1 kya).

³ pH of field soils (prior to LiCl saturation) measured in a paste comprising 1:1 mass ratio of soil to deionized water.

⁴ Organic carbon content of LiCl pastes measured by high temperature combustion and infrared CO₂ detection using a Shimadzu TOC-V CSH analyzer.

⁵ Mineralogy of soil clay fraction determined on the basis of x-ray diffraction, FTIR, and selective dissolution data. Upper case letters indicate major constituents, lower case letters indicate minor constituents; P = plagioclase; A = short-range-ordered Al gels or aluminosilicates (e.g., allophane); F = ferrihydrite; Q = quartz; V = vermiculite; HIV = hydroxyl-interlayered vermiculite; K = kaolin minerals (kaolinite and/or halloysite); Gi = gibbsite; He = hematite; Go = goethite; M = magnetite.

⁶ Structural (permanent) charge density determined using the Cs adsorption method (Anderson and Sposito, 1991; Chorover et al., 1999a).

Lyle, 1983; Aiken et al., 1985), which become intimately associated with soil minerals through interacting processes of mineral weathering and humification (Huang and Schnitzer, 1986).

Mineral-adsorbed SOM can modulate the surface chemistry of soil particles by masking the charge properties of underlying mineral colloids and reducing the variability in charge that is expected on the basis of heterogeneous mineral composition (Davis, 1982; Hunter and Liss, 1982; Beckett and Le, 1990; Chorover and Sposito, 1995b). However, the architecture of mineral-OM composites in volcanic ash soils is not confined to organic coatings on mineral surfaces. In soils comprising high concentrations of reactive Al and Fe, complexation with monomeric, polymeric, and colloidal hydroxy-metal species promotes coagulation and immobilization of SOM in the soil solid phase (Skjemstad, 1992; Jones and Bryan, 1998). These processes also contribute to the stabilization of SOM against decomposition (Torn et al., 1997) and to the extraordinary accumulation of organic C to nearly 40% of the total soil dry mass in some volcanic ash soils (Shoji et al., 1993; Wada, 1995; Chorover, 2002). In turn, SOM tends to decrease the rate at which minerals such as allophane and ferrihydrite transform to long-range ordered, crystalline solids, and thereby enhances the metastability of these PC phases. The change in surface charge of soil particles over the course of pedogenesis in basalt is certainly impacted by this coupling of mineral transformation and SOM retention, but there are no published studies that have provided an appropriate quantitative analysis of this process. The objectives of the present work were (i) to establish the relationships between parent material age, soil constituents, and

particle surface charge in a well-characterized chronosequence of humid tropical soils derived from Hawaiian basalt (Vitousek et al., 1997; Hotchkiss et al., 2000); and (ii) to utilize the results to better understand the changing nature of mineral-organic complexes during pedogenesis.

2. EXPERIMENTAL METHODS

2.1. Background

Surface charge of soil particles can develop as a result of proton or other ion complexation at the particle surface and from isomorphous substitution within the crystal structure. Net total particle surface-charge, σ_p , (in units of moles of charge per kilogram of solid [mol_c kg⁻¹]) is the sum of four components (Sposito, 1998):

$$\sigma_p = \sigma_0 + \sigma_H + \sigma_{IS} + \sigma_{OS} \quad (1)$$

where σ_0 is the net permanent structural-charge density resulting from isomorphous substitutions; σ_H is the net proton surface-charge density resulting from the difference in surface excess (q) of H⁺ and OH⁻ ions ($q_H - q_{OH}$); σ_{IS} is the net inner-sphere complex charge density resulting from total charge of ions (excluding H⁺ and OH⁻) bound into inner-sphere surface coordination; and σ_{OS} is the net outer-sphere complex charge density resulting from total charge of ions (excluding H⁺ and OH⁻) bound into outer-sphere surface coordination. If σ_p is nonzero, then it must be balanced by charge of ions adsorbed in the diffuse layer, σ_D :

$$\sigma_p = -\sigma_D \quad (2)$$

The net charge of ions (excluding H⁺ and OH⁻) adsorbed into surface complexes and the diffuse ion swarm is given by the surface excess of cation minus anion charge (Δq , mol_c kg⁻¹):

$$\Delta q = (q_+ - q_-) = \sigma_{IS} + \sigma_{OS} + \sigma_D \quad (3)$$

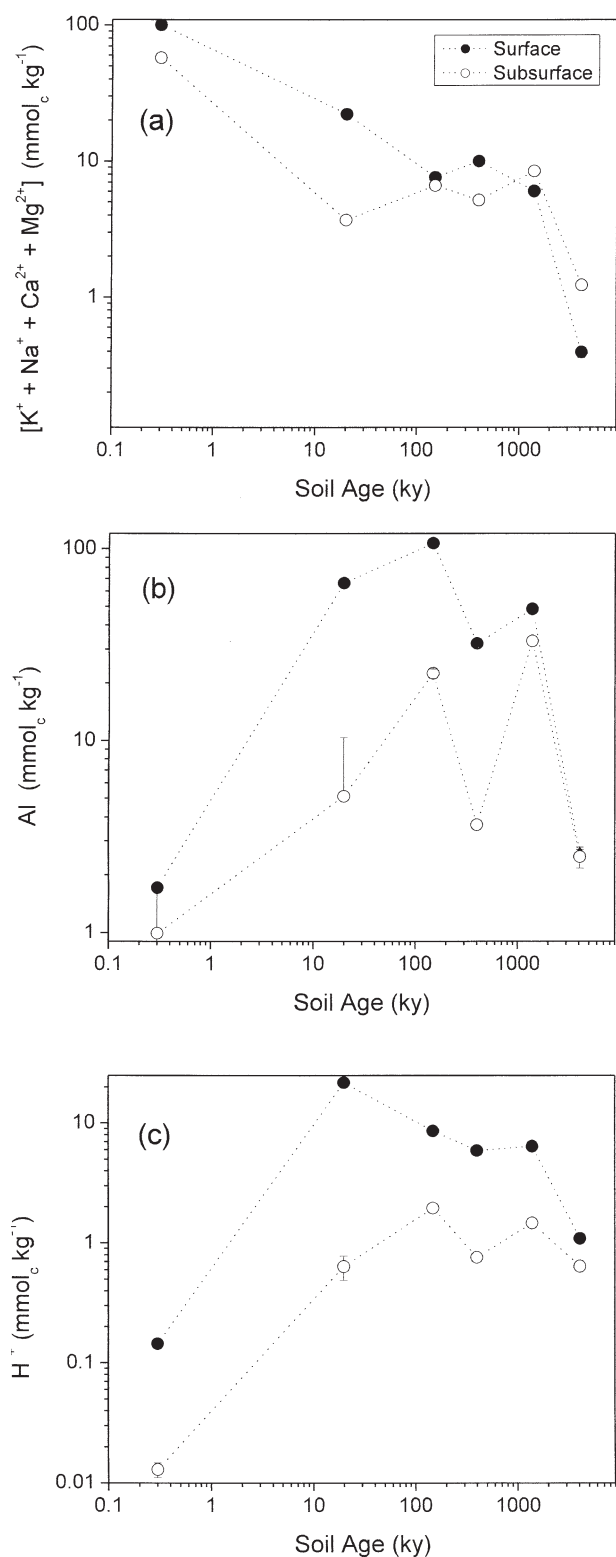


Fig. 1. Cation charge extracted during Li⁺ saturation of chronosequence soils: (a) sum of exchangeable non-hydrolyzing ("base") cations; (b) Al; and (c) H⁺. Error bars correspond to standard deviations of triplicate measurements (not shown if smaller than data symbol).

The *point of zero net charge* (PZNC) is defined as the pH value where Δq is equal to zero.

The surface charge balance requires that the intrinsic charge of soil particles, σ_{in} , including that resulting from both isomorphous substitutions (*permanent charge*) and proton adsorption (*variable charge*) must be balanced by adsorption from solution of background cation and anion:

$$\sigma_{in} = \sigma_0 + \sigma_H = -\Delta q \quad (4)$$

The *point of zero net proton charge* (PZNPC) is defined as the pH value where σ_H is equal to zero. Therefore, by Eqn. 4, this is the pH value where $\Delta q = -\sigma_0$. Experimental methods for measuring surface charge components in Eqn. 4 include *proton titration* for σ_H (Stumm, 1992), *preferential Cs⁺ adsorption* for σ_0 (Anderson and Sposito, 1991), and *background ion adsorption* for Δq (Sposito, 1998). Whereas σ_0 is constant for a given soil, σ_H and Δq vary with pH and ionic strength (*I*).

These surface charge components must be measured independently to assess conformation of the data to Eqn. 4 (Chorover and Sposito, 1995a). This is particularly important in whole soils comprising admixtures of PC minerals and organic matter where side reactions can diminish the accuracy of charge measurements. Adsorption and dissolution reactions both consume aqueous H⁺ or OH⁻; therefore, proton titration data must account for the stoichiometry of dissolution side reactions. Furthermore, re-adsorption of charged dissolution products (e.g., Al³⁺) can impact the surface excess of index ions used to measure adsorbed ion charge (Skylberg and Borggaard, 1998).

2.2. Chronosequence Field Sites and Sample Collection

Field-moist soil samples were collected from six sites along a well-characterized chronosequence on the islands of Hawaii, Molokai, and Kauai (Table 1), known as the "long substrate age gradient" or LSAG (Vitousek et al., 1997). Along the LSAG, variation in "state factors" of soil formation (Jenny, 1941) other than time (i.e., climate, biota, relief, parent material) have been kept to a minimum. Site locations, additional information on soil and ecosystem properties, and reconstruction of the long-term geomorphological/climatic history of the sites as related to their use as a "true chronosequence" are published elsewhere (Crews et al., 1995; Vitousek et al., 1997; Chorover et al., 1999a; Hotchkiss et al., 2000; Vitousek, 2004). One of the principal conclusions of these and related studies is that the LSAG covers such a long time span that variation in other state factor parameters, which could be problematic in shorter sequences, is minimized in terms of impact on LSAG pedogenesis.

All soils were formed from basaltic materials composed primarily of tephra (the sum of all volcanic pyroclastics) overlying lava or a lava-ash mixture (Torn et al., 1997) containing glass, olivine, clinopyroxene, feldspar, and magnetite-ilmenite (Vitousek et al., 1997). The LSAG includes Andisols that eventually weather to form Oxisols at advanced weathering stages. Soil classifications for each of the six sites (Table 1) are as follows: (1) Thaptic Udivitrand (Ola'a), (2–4) Aquic Hydrudand (Laupahoehoe, Kohala, Pololu), (5) Aquic Hapludand (Kolekole), and (6) Plinthic Kandiodox (Kokee). Each soil contains organic (O) horizons overlying organic-rich mineral horizons (A), subsoil B horizons (Bw), and partially weathered parent material (Cr). Buried horizons (resulting from periodic eruptions) are evident for some sites at depths greater than those studied here. All sites are located in montane rainforest dominated by the tree *Metrosideros polymorpha*, on level terrain at 1130 to 1500 m elevation, with mean annual soil temperature of 289 K, and mean annual precipitation of 2500 mm. All soils are derived from a mixture of volcanic tephra and lava, with tephra being the dominant parent material. Parent material age, measured using ¹⁴C and K/Ar radiometric techniques, ranges from 300 yr at the Ola'a site on the island of Hawaii to 4.1 × 10⁶ yr at the Kokee site on the island of Kauai (Table 1). Samples collected from pit faces were composited in the field and transferred into Ziploc bags, double bagged, and then transported to the laboratory in coolers maintained at low temperature by addition of ice packs. Samples were stored field-moist at 277 K before use.

Table 2. Major element concentrations in LSAG soils.

Soil Sample	Total (Li-metaborate fusion) ¹				Oxalate extractable ²			
	Si	Al	Fe	Ti	Si	Al	Fe	Ti
	(g kg ⁻¹)				(g kg ⁻¹)			
Surface (10–20 cm)								
Ola'a A	180 (3.4)	55.0 (2.7)	79.6 (4.9)	15.8 (0.8)	2.02 (0.10)	10.63 (0.76)	15.6 (0.7)	1.45 (0.11)
Laupahoehoe A	26.3 (1.2)	12.1 (0.8)	149.7 (8.5)	46.3 (2.8)	0.06 (0.004)	2.46 (0.28)	52.21 (2.4)	3.19 (0.10)
Kohala A	50.6 (2.8)	37.8 (1.1)	22.8 (2.2)	34.4 (1.2)	4.64 (0.07)	33.98 (0.36)	10.58 (0.76)	2.88 (0.09)
Pololu A	169 (6.1)	50.5 (3.9)	33.4 (1.7)	126.7 (7.6)	0.005 (0.004)	6.11 (0.04)	2.17 (0.02)	0.46 (0.01)
Kolekole A	127 (2.7)	43.7 (1.8)	129.4 (7.4)	105.4 (5.3)	0.01 (0.005)	1.89 (0.07)	17.49 (0.49)	0.13 (0.01)
Kokee A	52.3 (2.3)	14.1 (0.4)	314.0 (16.9)	159.4 (5.9)	n.d. ³	0.48 (0.02)	1.93 (0.07)	0.023 (0.00)
Subsurface (50–70 cm)								
Ola'a B	226 (8.7)	66.3 (3.2)	87.6 (3.5)	18.6 (0.6)	1.29 (0.20)	1.73 (0.19)	5.31 (0.04)	0.35 (0.01)
Laupahoehoe B	28.4 (1.4)	78.0 (4.9)	150.4 (9.5)	30.8 (0.7)	8.54 (0.42)	69.7 (3.3)	102.00 (5.1)	7.89 (0.52)
Kohala B	118 (7.9)	163.1 (7.6)	38.3 (1.8)	23.2 (1.4)	19.80 (0.19)	68.7 (17.1)	5.36 (0.40)	10.79 (0.92)
Pololu B	51.7 (3.5)	105.7 (5.1)	99.3 (5.2)	22.1 (2.1)	22.22 (4.91)	85.2 (0.74)	38.68 (8.0)	3.13 (0.67)
Kolekole B	124 (8.2)	173.0 (6.5)	79.7 (4.1)	18.4 (0.6)	2.74 (0.01)	16.6 (0.74)	7.58 (0.52)	0.12 (0.01)
Kokee B	42.8 (3.1)	102.5 (6.8)	288.0 (16.8)	81.6 (5.2)	n.d.	1.04 (0.02)	0.96 (0.05)	0.022 (0.004)

¹ Total elemental analysis by Li-metaborate fusion (Hossner, 1996).

² Selective dissolution of Li-saturated soil pastes by acid ammonium oxalate using the method of Jackson et al. (1986).

³ n.d. = not detected.

2.3. Preparation and Characterization of Homoionic Soils

Surface (A, 10–20 cm) and subsurface (B, 50–70 cm) horizons were selected for detailed studies of surface charge behavior. Adsorbed native ions were first exchanged with LiCl, a 1-1 background electrolyte with easily replaceable cation and anion, in a series of four washing steps. Sixty grams of field-moist soil were washed in triplicate with 0.2 kg of LiCl solutions of progressively decreasing *I* (0.5 M, 0.1 M, 0.05 M and 0.01 M) in 250 mL polypropylene copolymer (PPCO) centrifuge bottles. For each wash, the bottles were placed on an end-over-end shaker at 7 rpm for 30 min, followed by centrifugation at 13,000 relative centrifugal force (RCF) for 15 min. Supernatant solutions from each step were analyzed for pH by glass electrode and for “exchangeable” cation (K, Na, Ca, Mg, Al) concentrations by atomic absorption/emission spectrometry (Instrumentation Laboratories, Video 22) and inductively coupled plasma optical emission spectrometry (ICP-OES). The soil pellets were then mixed to produce a uniform paste, and the water content was determined by oven drying replicate subsamples at 383 K so that all subsequent measurements could be reported on a dry mass basis. Analysis of dissolution products indicated that colloidal dispersion and loss of particulate matter was negligible during preparation of the soil pastes.

The LiCl saturated pastes were subjected to several wet chemical and spectroscopic analyses. Total and “labile” metal concentrations were measured following Li-metaborate fusion (Hossner, 1996) and 0.1 M oxalic acid extraction in the dark at pH 4 (Jackson et al., 1986), respectively, using inductively coupled plasma-mass spectrometry (Perkin Elmer DRC II ICP-MS). Organic carbon content of LiCl pastes was measured by high temperature combustion and infrared CO₂ detection using a Shimadzu TOC-V CSH analyzer.

Crystalline (C) soil minerals were determined on the basis of X-ray diffraction (Phillips XRG-3000) analysis of (i) whole soils and (ii) the soil clay fraction subjected to solvation with Mg, glycerol, and K to differentiate the layer silicate clays (Whittig and Allardice, 1986; DiChiaro, 1998; Chorover et al., 1999a). Diffuse reflectance infrared Fourier transform (DRIFT) spectroscopy was used to assess time-dependent evolution of the soil solid phase and the emerging crystallinity of soil minerals. The method is sensitive to PC minerals of short-range-order (e.g., allophane, microcrystalline gibbsite, ferrihydrite) and their complexes with organic matter (Russell and Fraser, 1994). These solids, which are amorphous to X-ray diffraction, predominate in volcanic ash soils. DRIFT spectra were collected on LiCl saturated soils (3% by mass folded into IR grade KBr) before and after oxalate extraction. Spectra were obtained by averaging 350 to 500

scans using a Nicolet 560 Magna IR spectrometer operating at 4 cm⁻¹ resolution.

Humic acid (HA) was extracted from all of the surface soils according to IHSS protocol (Swift, 1996) in 0.1 M NaOH under N₂ (g) purge before de-ashing in HF-HCl, dialyzing against MilliQ water (SpectraPor 3500 MWCO, Spectrum Laboratories, Laguna Hills, CA) until Cl⁻ was not detected in the dialysate, and then freeze-dried. Purified HAs were analyzed by ¹³C cross-polarization magic angle spinning (CP MAS) nuclear magnetic resonance (NMR) spectroscopy on a Chemagnetics M-100 spectrometer at a frequency of 25.04 MHz (100 MHz for ¹H) with MAS at 3.5 kHz. A contact time of 1 ms, a 90° ¹H pulse width of 6.6 ms, and a pulse delay of 600 ms were used for all spectra. Approximately 30,000 to 90,000 scans were accumulated.

2.4. Surface Charge Components

A Cs⁺ adsorption method (Anderson and Sposito, 1991) was employed in triplicate to quantify the magnitude of permanent charge (σ_0) associated with 2:1 layer-type silicates. We previously conducted detailed studies of Cs sorption to LSAG soils (DiChiaro, 1998; Chorover et al., 1999a), but those soils were collected at a different sampling time, so the measurements were repeated in this study and similar values were obtained (Table 1).

The following discontinuous (batch) titration procedure was performed at 298 K, and two ionic strengths (*I*) over a range in *proton concentration*, measured as $-\log[H^+]$ with target values ranging from 2 to 9 for 10.0 mM LiCl, and 3 to 7 for 1.0 mM LiCl. Although these values are hereafter referred to as “pH,” it must be noted that reference is being made to proton concentration rather than activity, since use of the former circumvents the problem of unknown electrode junction potentials and eliminates the need for activity coefficient models for calculation proton and hydroxide adsorption. Duplicate subsamples of Li-saturated soil pastes equivalent to 410 mg of dry soil were equilibrated in solutions of LiCl/HCl or LiCl/LiOH (total suspension mass = 41.0 g) to achieve target values for pH. Titration “blank” samples containing equivalent amounts of acid/base were prepared without soil. The tubes were mixed by gentle rotation on an end-over-end shaker at 7 rpm for 3 h and then centrifuged at 27,000 RCF for 20 min. The supernatant solution was carefully aspirated by Pasteur pipette into acid-washed, 60 mL HDPE bottles. An Orion-Ross 8102 combination electrode was calibrated by Gran titration under N₂ (g) purge, in LiCl and the same *I* as a given titration experiment, to give direct measurements of proton concentration. A 5 mL aliquot of LiCl supernatant

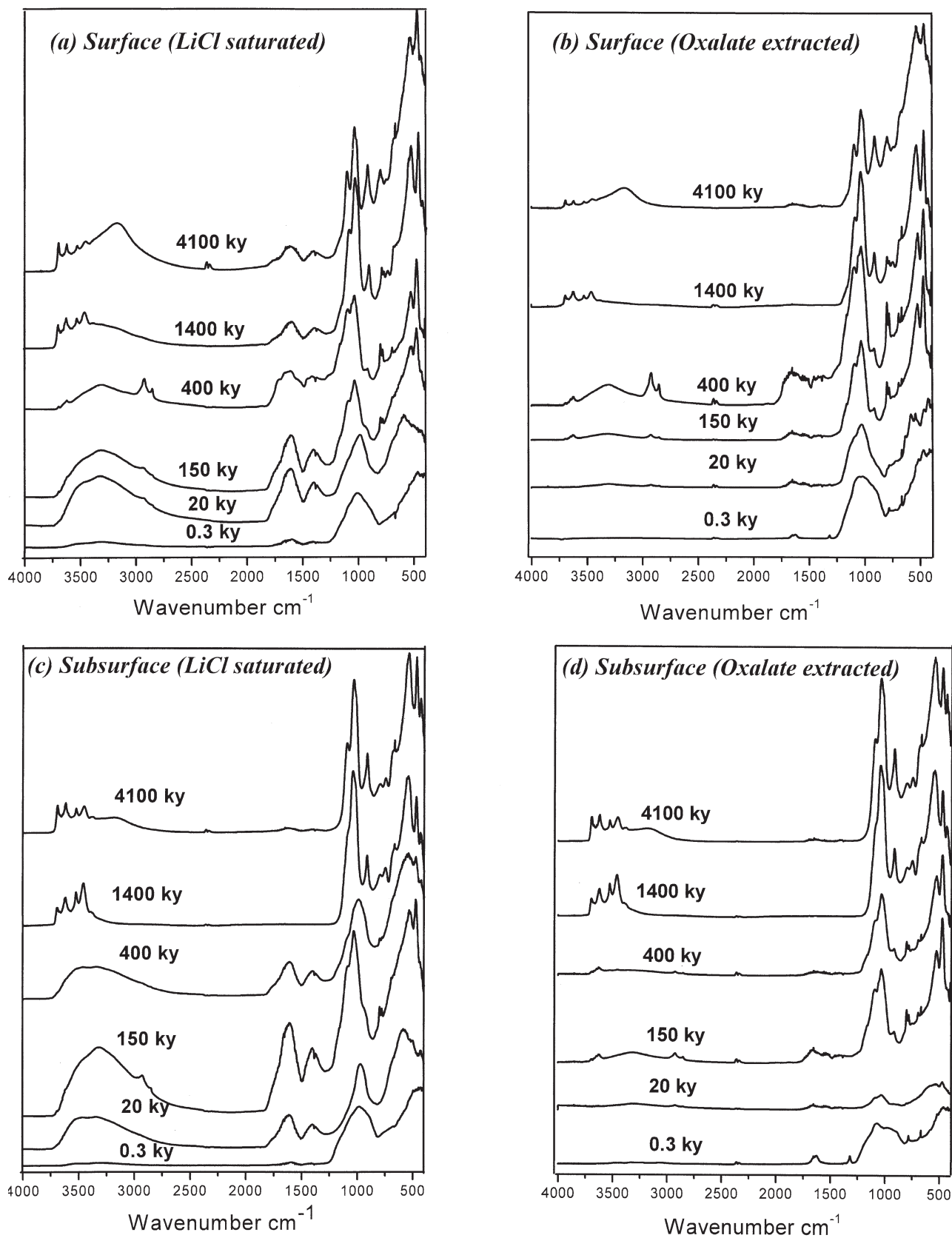


Fig. 2. Diffuse reflectance infrared Fourier transform (DRIFT) spectra of surface soils (a-b) and subsurface soils (c-d). For each pair of spectra, those on left (a or c) are whole soils after LiCl saturation. Spectra on right (b or d) are the same LiCl saturated soils that have been subsequently extracted in acid ammonium oxalate solution for 4 h.

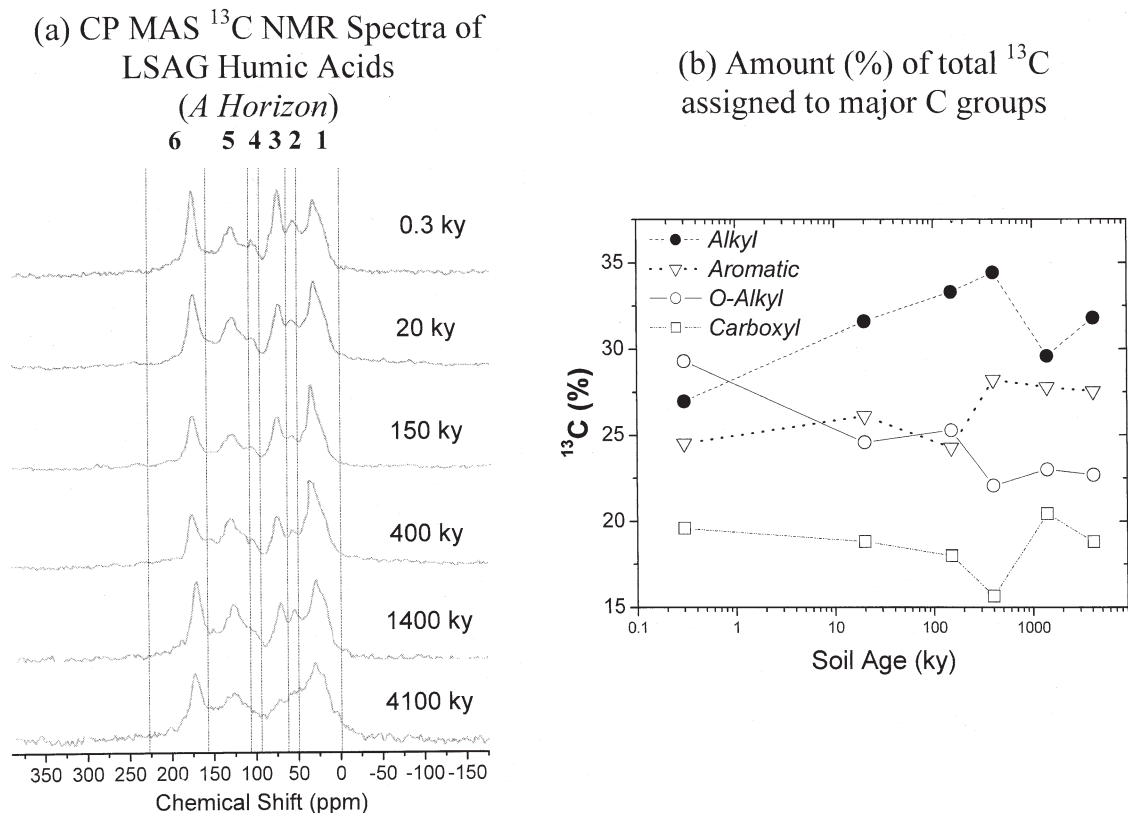


Fig. 3. (a) CP MAS ^{13}C -NMR spectra of humic acids extracted from the LSAG surface soils (chemical shifts relative to tetramethyl silane). Assignments for spectral regions 1 through 6 are provided in the text; (b) integrated spectral areas corresponding to major C functional groups.

solution was removed from each “blank” and reacted sample solution for immediate determination of $[\text{H}^+]$. Another 5 mL aliquot was Gran titrated to pH 2.5 with standardized HCl to obtain a measure of acid neutralizing capacity (ANC) associated with dissolved organic acids (Morel and Hering, 1993). The mass of each tube and its contents was recorded, and the mass of entrained solution was calculated by difference after correcting for the dry mass of soil. Adsorbed ions were then extracted by resuspending soil pellets in 40 mL of 1 M NH_4NO_3 for 30 min on a reciprocal shaker. The suspensions were centrifuged at 27,000 RCF for 10 min and the supernatant solutions were aspirated into 125 mL HDPE bottles. These extraction steps were repeated to ensure quantitative removal of adsorbed ions, and the extractant supernatant solutions were combined. The “LiCl supernatant” and “ NH_4NO_3 extractant” solutions were stored at 277 K before analysis by ICP-AES (Thermo Jarrell Ash Model 61 E, Franklin MA) to determine the concentrations of index cation (Li^+) and background metals resulting from dissolution. The index anion (Cl^-) was measured by ion chromatography. Dissolved organic carbon (DOC) in the LiCl supernatant solution was measured by high temperature combustion and infrared CO_2 detection using a Shimadzu TOC-V CSH (Columbia, MD).

2.5. Data Analysis

The surface excess (q) of ion i , in $\text{mol}_c \text{ kg}^{-1}$ of dry adsorbent, following 3 h reaction was calculated from:

$$q_i = z_i n_i (\text{NH}_4\text{NO}_3) - M_{\text{ent}} z_i m_i \quad (5)$$

where z_i is the valence of ion i , n_i , (NH_4NO_3) is the number of moles of ion i per unit dry soil mass extracted in the NH_4NO_3 step, M_{ent} is the mass of entrained LiCl solution per unit dry soil mass, and m_i is the moles of species i per unit mass of supernatant solution. Surface excess values were calculated for index cation Li^+ (q_+) and index anion Cl^-

(q_-), and the net adsorbed ion charge density, Δq , was calculated by Eqn. 3. Although the surface excess of Li^+ dominated the value of adsorbed cation charge, smaller quantities of bivalent ions (Ca^{2+} , Mg^{2+} , and Mn^{2+}) were observed and were included in the calculation of Δq . Values of adsorbed Al (q_{Al}) charge were calculated from Eqn. 5, with z_i (the charge on aquo Al and hydroxo-complexes at the experimental pH of the LiCl background solution) determined from speciation calculations using the thermo.dat database in *The Geochemist's Workbench* (Delany and Lundeen, 1989; Bethke, 2001).

The apparent proton surface charge density, $\sigma_{\text{H,titr}}$ was calculated for each pH value from the difference between the final $[\text{H}^+]$ and $[\text{OH}^-]$ of a sample and corresponding blank, corrected for proton consumption resulting from sorbent dissolution:

$$\sigma_{\text{H,titr}} = M_{\text{soln}} \left\{ ([\text{H}^+]_b - [\text{H}^+]_s) - \left(\frac{K_{\text{wc}}}{[\text{H}^+]_b} - \frac{K_{\text{wc}}}{[\text{H}^+]_s} \right) + (-z_{\text{avg}} \sum [c_i]_{\text{H}^+, \text{dissoln}}) \right\} \quad (6)$$

where M_{soln} is the mass of background electrolyte solution per unit dry adsorbent mass, $[\text{H}^+]$ is the concentration of protons in solution (mol kg^{-1}), and K_{wc} is the conditional dissociation product of water at the experimental I . The subscripts s and b denote sample and blank, respectively. The correction for the consumption of H^+ resulting from Al, Si, or Fe dissolution was made by multiplying the average valence, z_{avg} (valence weighted by the concentration of each species), which varies with pH and degree of hydrolysis, by the total free aqueous concentration of a given element. The correction is negative for proton promoted dissolution (i.e., pH < point of minimum dissolution) as indicated by the term $-z_{\text{avg}} \sum [c_i]_{\text{H}^+, \text{dissoln}}$. Aqueous speciation was calculated using Bethke (2001). No correction was made for pH > point

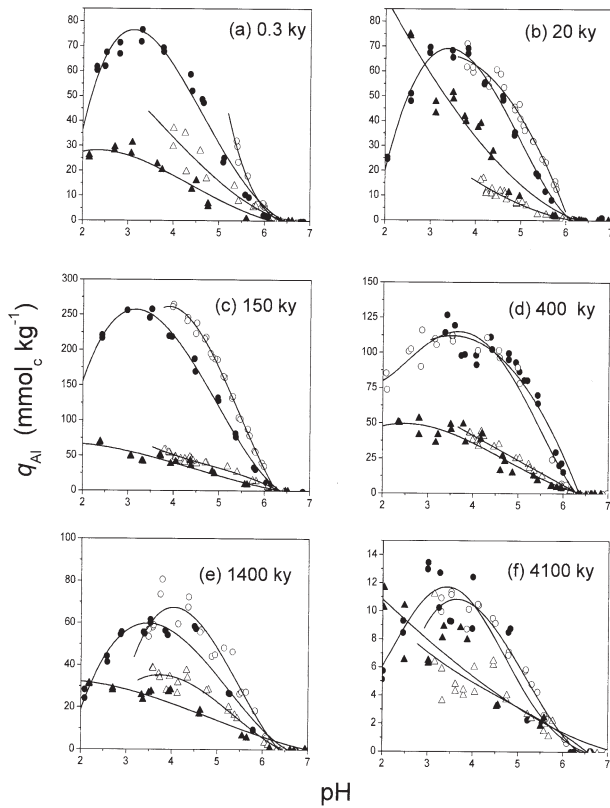
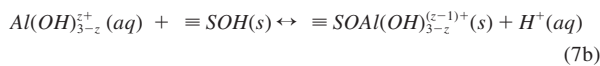


Fig. 4. Adsorbed Al charge calculated according to Eqn. 5, where z_i is the mean charge on aquo Al and hydroxo-complexes at the experimental pH of the LiCl background solution. Surface soils: [circo] = 1 mM LiCl; \bullet = 10 mM LiCl. Subsurface soils: Δ = 1 mM LiCl; \blacktriangle = 10 mM LiCl. Note that Y axis scales vary with soil age.

of minimum dissolution because at this pH, metal release was also promoted by dispersion of metal-organic complexes rather than only by classic proton or hydroxide promoted dissolution mechanisms.

Particle readsorption of dissolved Al was found to be significant (not so for Fe and Si), as indicated from measurements of Al surface excess (Eqn. 5; also see section 3.3). The sequence of dissolution and adsorption reactions may be written using dissolution of solid phase gibbsite as an example:



Here, $Al(OH)_{3-z}^{z+}(aq)$ is the aquo or hydroxo Al species (with a valence of z) in solution, $\equiv SOH(s)$ represents an adsorption site, and (aq) and (s) represent the aqueous and solid phases, respectively. Thus, the proton mass balance used to calculate σ_H is corrected (as in Eqn. 6) for H^+ consumption that results in aqueous phase Al (i.e., dissolution only, Eqn. 7a), whereas no correction is applied for the measured mass of adsorbed Al, since adsorption (Eqn. 7b) results in an increase in particle surface charge that exactly balances the moles of protons consumed in the combined dissolution reabsorption reaction. This approach treats the reabsorbed Al as a potential determining ion that is analogous to H^+ and also one that should affect the pH-dependent adsorption of index cation (Li^+) and anion (Cl^-). For example, formation of Al surface complexes as depicted in Eqn. 7b should affect background ion adsorption through pH dependent hydrolysis reactions of $\equiv SOAl(OH)_{3-z}^{(z-1)+}(s)$ groups.

The net proton surface charge density, σ_H , for a given pH and I is defined as the difference between the apparent proton surface charge

density at that pH and the apparent proton surface charge density at the PZNPC (Chorover and Sposito, 1995a):

$$\sigma_H(pH, I) \equiv \sigma_{H, \text{titr}} - \sigma_{H, \text{titr}}(\text{PZNPC}, I) \quad (8)$$

From Eqn. 4,

$$\sigma_H(pH, I) = -\Delta q - \sigma_0 \quad (9)$$

and, therefore

$$\sigma_{H, \text{titr}}(\text{PZNPC}, I) = \sigma_H(pH, I) + \sigma_0 + \Delta q \quad (10)$$

A value for the right side of Eqn. 10 was calculated for each titration point at a given I and an average value of $\sigma_{H, \text{titr}}(\text{PZNPC}, I)$ was taken as the mean. The PZNC and PZNPC values for each soil and I were calculated by fitting Δq and σ_H data to quadratic functions of pH and solving for pH in the resultant function for the conditions $\Delta q = 0$ and $\sigma_H = 0$, respectively.

3. RESULTS

3.1. Bulk Soil Chemistry and Mineralogy

Upon collection (before saturation with LiCl), surface soils exhibited lower pH than those collected from the subsurface (Table 1). They also had higher organic C contents (Table 1) and Li^+ exchangeable acidity (Al and H^+) (Fig. 1). There is a large decrease in the concentration of adsorbed nonhydrolyzing cations (K^+ , Na^+ , Ca^{2+} , Mg^{2+}) with increasing parent material age (referred to hereafter as “soil age”), whereas moles of exchangeable Al and H^+ charge appear to be highest for the intermediate-aged soils (Fig. 1).

Selected chemical and mineralogical data on the LiCl saturated soils are presented in Tables 1 and 2. Mean values are followed by their standard deviations in parentheses. Mineralogical composition of each soil sample, based on XRD (high resolution X-ray diffraction), DRIFT, and chemical extraction results, is reported in Table 1. Results of dissolution analyses, for both Li-metaborate fusions and oxalate extractions, are presented in Table 2.

3.2. Spectroscopic Analyses of the Soil Solid Phase

3.2.1. DRIFT spectra of LiCl saturated whole soils

Figure 2 shows DRIFT spectra of surface soils (a) *before* and (b) *after* acid oxalate extraction (oxalate removed after reaction by washing in LiCl), and the same is shown for subsurface soils in Figure 2 (c) and (d). At early weathering stage (0.3–20 ky), the O-H stretching vibrations ($3700\text{--}3000\text{ cm}^{-1}$) that correspond to structural O-H of minerals and phenolic O-H of organic matter increase in intensity to form a single broad band by 20 ky. The broad band, resulting predominantly from PC minerals (allophane, Al, Fe-gels) and organic matter, persists through intermediate weathering stage (150 and 400 ky). At 400 ky, sharper O-H peaks are just beginning to emerge at the higher frequency end of the O-H band in the surface soil (Fig. 2a), but not yet in the subsurface (Fig. 2b). These bands become more pronounced in both surface and subsurface 400 ky soils after selective dissolution in oxalate (Fig. 2b and 2d), and they are also visible after oxalate reaction—even for the 150 ky site, whereas the broad O-H stretch associated with PC Al, Si, and Fe bearing solids is removed upon oxalate treatment. The emergent peaks, at 3697 , 3623 , 3527 , and 3460 cm^{-1} , become well-defined at advanced weathering stages (1400–4100 ky) in both surface and subsurface soils, along with a broad

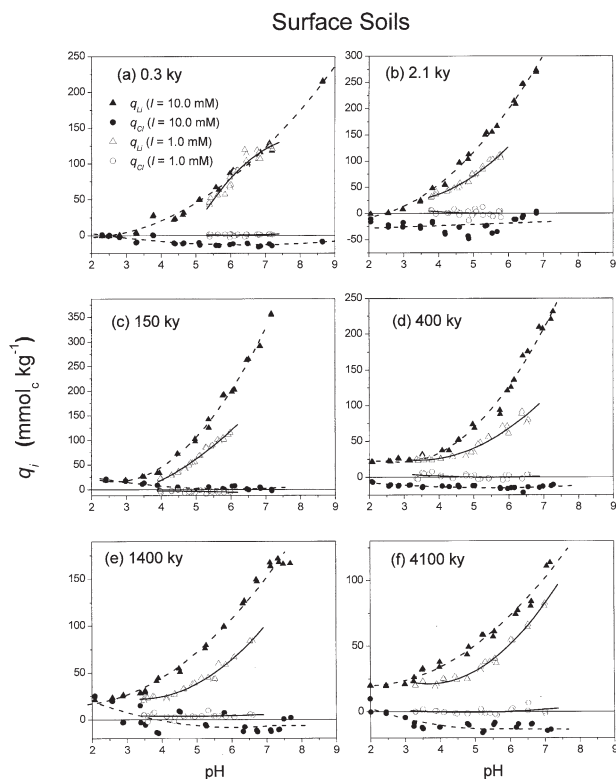


Fig. 5. Surface excess of Li^+ and Cl^- on **surface soils** plotted as a function of pH and I . Adsorption of Li^+ and Cl^- is indicated by triangles and circles, respectively. Filled and open symbols correspond to 10.0 mM and 1.0 mM LiCl, respectively. Note that Y axis scales vary with soil age.

peak centered at 3200 cm^{-1} , corresponding to the phenolic OH stretch (Baes and Bloom, 1989) (Fig. 2). The 3697 and 3623 cm^{-1} peaks are consistent with kaolin (kaolinite and/or halloysite) (Farmer, 1974); the first sign of kaolin is in the oxalate-treated 150 ky soils. Peaks at 3527 and 3460 cm^{-1} are diagnostic of gibbsite (Hsu, 1989). The kaolin and gibbsite peaks persist after the oxalate reaction, attesting to the slower kinetics of dissolution of these solids relative to PC materials.

Through the 400 ky soil, the Si(Al)-O-Si(Al) stretching region, which is manifest as a broad band that extends from 1250 to 815 cm^{-1} , is consistent with a prevalence of PC allophane and hydrous oxides of Al and Fe (Harsh et al., 2002). With increasing soil age, individual peaks become better defined, such that by 4100 ky, three distinct peaks are observed: the asymmetric (1097 and 1037 cm^{-1}) and symmetric (914 cm^{-1}) stretches show narrowing bandwidth and increased definition with increasing soil age and mineral crystallinity. The doublet peak at 800 and 781 cm^{-1} is characteristic of quartz, (confirmed by XRD), which is of eolian origin and derives from Asia (Jackson et al., 1971; Kurtz et al., 2001). Vibrations of Fe-O bonds contribute to the broader absorbance at $840\text{--}790\text{ cm}^{-1}$, the peak at 670 cm^{-1} (asymmetric stretch) and at $420\text{--}400\text{ cm}^{-1}$ (symmetric stretch) (Cornell and Schwertmann, 1996). The weathering stage-dependent accumulation and then diminution of PC minerals is further supported by the mass of oxalate extractable major elements relative to their total mass in the LSAG samples (Table 2). The fraction of soil Al, Fe, Si, and

Ti that is extractable in oxalate is highest for the intermediate (150 and 400 ky) age soils and decreases thereafter.

The bands centered at 1650 and 1400 cm^{-1} result primarily from soil organic matter (SOM). Asymmetric and symmetric stretching of carboxylate contribute to these bands respectively, as does aromatic C = C stretching and HOH deformation of adsorbed water associated with hydrous minerals (1640 cm^{-1}), and $-\text{CH}$ bending (1400 cm^{-1}) (Baes and Bloom, 1989). The strong SOM absorbances observed at both depths for the 20, 150, and 400 ky soils (Fig. 2a and 2c) are greatly diminished upon oxalate treatment (Fig. 2b and 2d), indicating that selective dissolution of amorphous solids leads to solubilization of SOM. The broad band at 1030 cm^{-1} and shoulder at 1100 cm^{-1} correspond to the Si-O stretch of silicates and C-O stretching of polysaccharides. The peak at 915 cm^{-1} emerges in the two oldest soils. Peaks at 526 and 474 cm^{-1} are assigned to Al-O and Fe-O stretching, respectively. Overall, despite enhancement of SOM absorbances in surface soils, DRIFT spectral differences between surface and subsurface horizons are small relative to differences between sites.

3.2.2. NMR spectra of soil humic acids (HAs)

The CP MAS ^{13}C -NMR spectra for HAs extracted from the surface soils (Fig. 3a) show six principal peaks corresponding to (1) unsubstituted aliphatic C comprising methyl, methylene, and methine groups, e.g., of fatty acids, waxes and resins (0 to 10

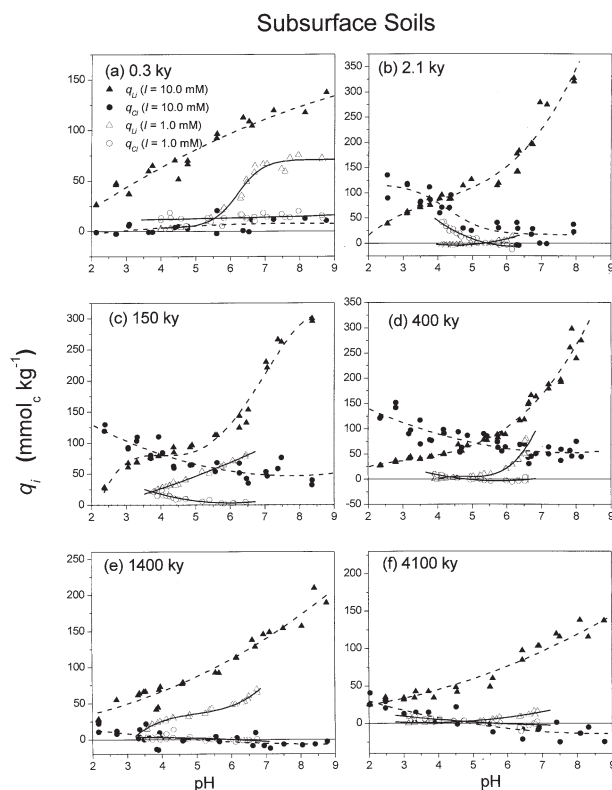


Fig. 6. Surface excess (q) of Li^+ and Cl^- on **subsurface soils** plotted as a function of pH and I . Adsorption of Li^+ and Cl^- is indicated by triangles and circles, respectively. Open and filled symbols correspond to 1.0 mM and 10.0 mM LiCl, respectively. Note that Y axis scales vary with soil age.

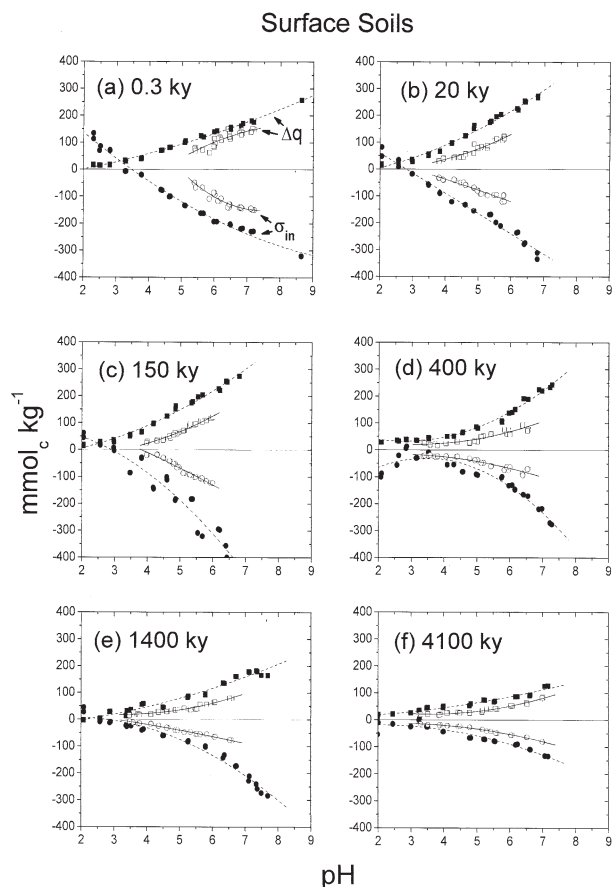


Fig. 7. Surface charging curves for **surface soils** showing the pH-dependent balance between net adsorbed ion charge (Δq , squares) and intrinsic surface charge (σ_{in} , circles) measured as a function of pH. Open and filled symbols correspond to 1.0 mM and 10.0 mM LiCl, respectively. Data intersection with the horizontal line indicates the point of zero net charge ($\sigma_{in} = \Delta q = 0$). Intrinsic surface charge density includes both structural and proton charge components (Eqn. 4).

ppm); (2) C in C-O of methoxyl groups (50 to 60 ppm); (3) C in other aliphatic C-O and C-N groups, including oxygenated C from phenyl propanoid units of lignin, as well as carbohydrate C (60 to 95 ppm); (4) anomeric C (small shoulder, 95 to 110 ppm); (5) aromatic C (110 to 160 ppm); and (6) carbonyl in carboxyl, ester and amide groups (160 to 230 ppm) (Preston and Blackwell, 1985; Malcolm, 1989). The carbonyl peaks in all LSAG HA spectra extend from 160 to 190, which indicates that this peak derived principally from carboxyl, and we label it as such in Figure 3b (Malcolm, 1989; Kögel-Knabner et al., 1991), where results of peak integration are reported. The range above baseline from 0 to 60 ppm (regions 1 plus 2) was combined for quantification of alkyl C and from 60 to 110 ppm (regions 3 plus 4) for quantification of O-alkyl C (Hatcher et al., 1981a; Hatcher et al., 1981b; Preston, 1996).

3.3. Proton Titration Experiments

3.3.1. Adsorption of Al

Although some dissolution of Fe and Si was observed, they exhibited much lower solubility than Al, and their readsorption,

as measured by Eqn. 5, was negligible. In contrast, readsorption of Al was significant. The surface excess of Al charge is plotted for each soil as a function of pH and I (1 or 10 mM) in Figure 4. Values of q_{Al} for surface soils increased with pH from pH 2 to a $q_{Al,max}$ near pH 3.0 to 4.5 (depending on soil and I), then decreased sharply to pH 6.5, and were higher overall than values for subsurface soils. For a given surface soil, $q_{Al,max}$ is shifted to higher pH, and q_{Al} is higher (for a given pH), at lower I (except for 20 ky subsurface) because of diminished sorptive competition with background Li^+ . A $q_{Al,max}$ is less evident for the subsurface soils, many of which show an increase in q_{Al} with decreasing pH throughout the range of measurement. Since titration experiments extended to pH values lower than encountered in the field soils, maximum values of q_{Al} after the 3 h reaction time (Fig. 4) sometimes exceeded the moles of Al displaced during LiCl saturation of the field soils (Fig. 1c). Also, an unknown fraction of n_{Al} , (NH_4NO_3) derives from mineral dissolution during the extraction. At pH >7, q_{Al} was negligible for both surface and subsurface soils.

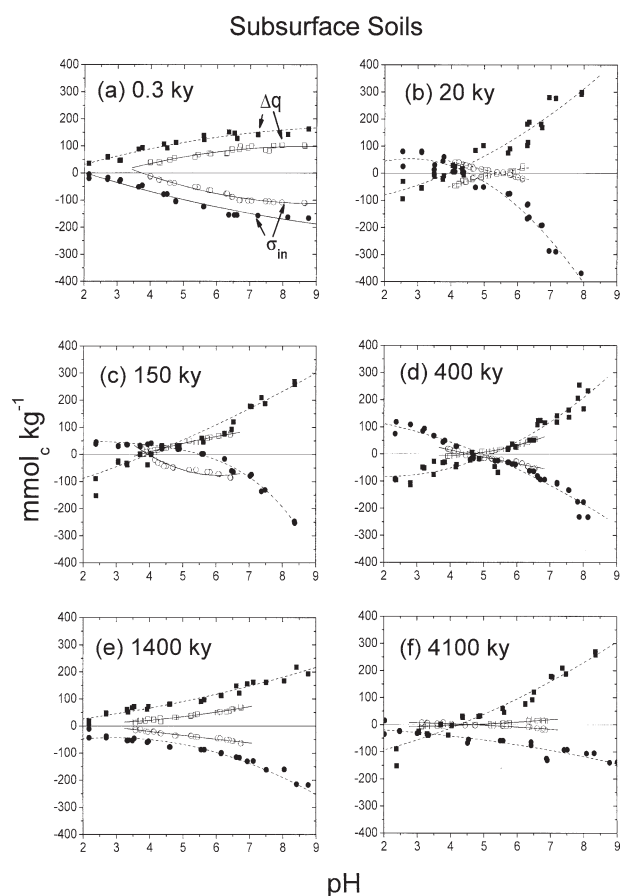


Fig. 8. Surface charging curves for **subsurface soils** showing the pH-dependent balance between net adsorbed ion charge (Δq , squares) and intrinsic surface charge (σ_{in} , circles) as a function of pH. Open and filled symbols correspond to 1.0 mM and 10.0 mM LiCl, respectively. Data intersection with the horizontal line indicates the point of zero net charge ($\sigma_{in} = \Delta q = 0$). Intrinsic surface charge density includes both structural and proton charge components (Eqn. 4).

Table 3. Summary of surface charge balance regression data (Δq versus σ_H). Regression slope and intercept confidence intervals ($p = 0.05$) are indicated in parentheses. All R^2 are significant at $p < 0.0001$.

	$I = 0.001$			$I = 0.01$		
	Slope (\pm c.i.)	Intercept (\pm c.i.) (mmol _c kg ⁻¹)	R ²	Slope (\pm c.i.)	Intercept (\pm c.i.) (mmol _c kg ⁻¹)	R ²
Surface (10–20 cm)						
Ola'a A	-0.76 (0.17)	74 (11)	0.790	-0.54 (0.063)	80 (5)	0.931
Laupahoehoe A	-1.00 (0.18)	51 (6)	0.858	-0.77 (0.104)	67 (14)	0.908
Kohala A	-0.84 (0.07)	63 (2)	0.970	-0.87 (0.052)	72 (7)	0.983
Pololu A	-1.02 (0.08)	92 (5)	0.970	-0.87 (0.140)	93 (10)	0.874
Kolekole A	-0.89 (0.15)	28 (3)	0.880	-0.66 (0.072)	46 (9)	0.925
Kokee A	-1.02 (0.16)	15 (4)	0.882	-0.8 (0.118)	23 (8)	0.868
Subsurface (50–70 cm)						
Ola'a B	-0.62 (0.06)	82 (2)	0.938	-0.70 (0.068)	86 (5)	0.953
Laupahoehoe B	-1.02 (0.08)	17 (3)	0.972	-0.81 (0.093)	31 (14)	0.928
Kohala B	-1.06 (0.21)	61 (3)	0.946	-1.00 (0.190)	111 (18)	0.839
Pololu B	-0.85 (0.09)	26 (2)	0.943	-1.00 (0.087)	36 (9)	0.963
Kolekole B	-1.05 (0.13)	31 (1)	0.937	-0.98 (0.127)	39 (10)	0.925
Kokee B	-0.98 (0.22)	4 (1)	0.776	-1.14 (0.182)	-8 (17)	0.88

3.3.2. Background ion adsorption

Values of surface excess (q) for index cation (Li^+) and anion (Cl^-) show significant pH and I dependence for both surface and subsurface soils. Adsorption edges for Li^+ in the surface soils are convex, with an increase in slope above pH 3.5 to 4.0 at high I , and above 4.0 to 5.0 at low I (Fig. 5). The pH value of changing slope corresponds with the onset of a decrease in q_{Al} (Fig. 4), signaling the important contribution of adsorbed Al to positive surface charge at low pH. In the surface soils, decreasing I results in a decrease in q_{Li} and a slight increase in q_{Cl} (except for the 150 ky soil, Fig. 5c, where effect of I on q_{Cl} is insignificant). At 10 mM LiCl , q_{Cl} is negative (i.e., anion exclusion) for surface soils throughout much of the pH range, and it is consistently near zero at 1 mM LiCl . In general, q_{Cl} exhibits smaller pH dependence than does q_{Li} , and only slight increases in adsorption occur with decreasing pH in the surface soils.

Adsorption of Cl^- is significantly enhanced in the subsoil, positive surface excess values are observed at acidic pH in most cases and q_{Cl} shows greater dependence on pH, particularly in the 20 to 400 ky soils (Fig. 6). For the intermediate-aged soils that are enriched in PC solids (20, 150, and 400 ky), the increase in slope for the Li^+ adsorption edge is shifted to higher pH than for the surface soils. In contrast to the case for the surface soils where adsorbed cation charge increases and adsorbed anion charge decreases with increasing I , both q_{Li} and q_{Cl} increase with ionic strength in the 20, 150, and 400 ky subsoils.

3.3.3. Balance of surface charge

According to Eqn. 4, the intrinsic surface charge density ($\sigma_{\text{in}} = \sigma_H + \sigma_0$) is equal in magnitude and opposite in sign to the net adsorbed ion charge density ($\Delta q = q_{\text{Li}} - q_{\text{Cl}}$). Plots of σ_{in} and Δq vs. pH for surface soils (Fig. 7) and subsurface soils (Fig. 8) show the response of soil surface charge to changes in I and pH. Second order polynomial best fits are provided as lines through the data. The σ_{in} curves show all of the structure of the proton titration data, since every data point differs from σ_H only by the constant value of structural charge given in Table 1. These independent data sets for

proton titration and ion adsorption may be used to evaluate their correspondence. In principal, the data sets should be mirror images of each other across the x -axis, with σ_{in} a decreasing (and Δq an increasing) function of pH, and an intersection point at the PZNC, where $\sigma_{\text{in}} = \Delta q = 0$. Deviations are interpreted as experimental error.

Taken as a whole, Figures 7 and 8 provide characteristic *surface charging signatures* across the LSAG. Since all curves are drawn to identical scale, age- and depth-dependent changes in slope and concavity of the curves are readily apparent. Charging curves for the youngest (0.3 ky) site (Figs. 7a and 8a) show a decreasing rate of charge development with increasing pH (i.e., concave toward the x -axis) for both depths, and the slopes decrease from surface to subsurface. The pH dependence of surface charging increases in magnitude with increasing soil age and the curves become convex (i.e., concave away from the x -axis), before decreasing in magnitude for the older sites.

In accordance with Eqn. 4, a stringent test of surface charge balance involves linear regression of σ_H against Δq , which should give a slope equal to -1 and an intercept equal to $-\sigma_0$, irrespective of soil or I (Chorover and Sposito, 1995a). Regression results across all experiments are given in Table 3, along with 95% confidence intervals for slope and intercept. At low I , slopes and intercepts are not statistically different from -1 and $-\sigma_0$, respectively, in eight of the twelve regressions. Exceptions include the 0.3 ky (Ola'a surface and subsurface) soils, where slope magnitude was less than 1 and intercept magnitude was larger than $|\sigma_0|$. The slope magnitude was underpredicted by 16% for the 150 ky (Kohala) surface soil and by 15% for the 400 ky (Pololu) subsurface soil. At the higher I , slight underprediction of slope is reported in all but one of the surface soils and only two of the subsurface soils (Table 3).

4. DISCUSSION

4.1. Dissolution of Organic C

Data extend over a larger pH range at high I relative to low I (Figs. 7 and 8). Underprediction of σ_H vs. Δq slope at high I

(Table 3) suggests that, in addition to adsorption of H^+ (low pH) or OH^- (high pH), other side reactions are contributing to proton or hydroxide consumption. Given that (i) values of σ_H were corrected for mineral dissolution (Eqn. 6) and (ii) the greatest discrepancies are observed in the surface soils, we postulated that some H^+ and OH^- consumption occurred in conjunction with dissolution of organic matter. DOC release into the LiCl supernatant solutions was found to be pH dependent, with a point of minimum dissolution (p.m.d.) between pH 3 and 4.5 depending on the soil, increasing modestly below—and more significantly above—the p.m.d. (Fig. 9). DOC concentrations were higher for surface than subsurface soils and increased significantly at pH >6. Deviation of the sum ($\sigma_{in} + \Delta q$) from zero followed a similar trend, suggesting correlation. Regression of ($\sigma_{in} + \Delta q$) ($mmol_c kg^{-1}$) against DOC (in units of $g kg^{-1}$ soil) for pH >3.5 indicates that 2 to 8 mmoles of charge are consumed per gram of C released. ANC measurements of LiCl supernatant solutions likewise indicated that titratable charge of DOC ranged from 1 to 10 $mmol_c g^{-1}$ C. These values for DOC charge are in agreement with those reported for the carboxyl acidity of DOM (Perdue and Lytle, 1983). Skjellberg and Borggaard (1998) also reported a significant effect of organic C dissolution on calculated values of σ_H for Spodosol horizons. Therefore, proton and hydroxide promoted release of DOC accounts for the deviation from unit slopes in the surface charge balance regression data (Table 3). That is, the magnitude of σ_H , as calculated from Eqn. 8, is overestimated by an amount equivalent to the charge consumed in dissolving organic matter. The effect is significant for organic-rich surface soils at high pH (and therefore most important at high I) (Table 3). Hence, the background ion adsorption (Δq) data provide a more accurate measure of particle surface charge when the two results are not in perfect agreement.

4.2. Charging of Soils Across the LSAG

4.2.1. Structural charge

In a prior study, we detected small quantities of structurally charged vermiculite and hydroxy-interlayered vermiculite (HIV) in LSAG soils using high resolution X-ray diffraction (XRD); peak intensities for the 2:1 layer silicates were correlated with structural charge densities measured by the Cs^+ adsorption method (Chorover et al., 1999a). Although the present study employs soils collected from the same LSAG sites, sample collection was performed at a different time, so that measurements of structural charge density had to be repeated. The values of structural charge (σ_o) for the present study (Table 1) are similar in magnitude to those reported in the prior work (Chorover et al., 1999a). The data reveal an accumulation of 2:1 layer silicates with soil age up to intermediate weathering stage (150–400 ky), followed by a decrease thereafter. As discussed in Chorover et al. (1999a), this pattern reflects either a pedogenic origin (Wada and Aomine, 1973; Shoji et al., 1981) or eolian delivery (Dymond et al., 1974; Kurtz et al., 2001), and its impact is greatest in the surface horizon.

4.2.2. Slopes of the charging curves

Although quadratic functions provide a useful guide to the eye for data in Figures 7 and 8, linear regression against pH gives mean regression coefficient (R) values of 0.95 (ranging from 0.85 to 0.99) for σ_H and 0.96 (ranging from 0.88 to 0.99) for Δq ($p < 0.001$). The goodness of linear fit over the wide range in pH is consistent with the lack of clear breaks in slope in the charging curves (Fig. 7 and 8). Evidently, charge development occurs on dissociable surface sites that together give

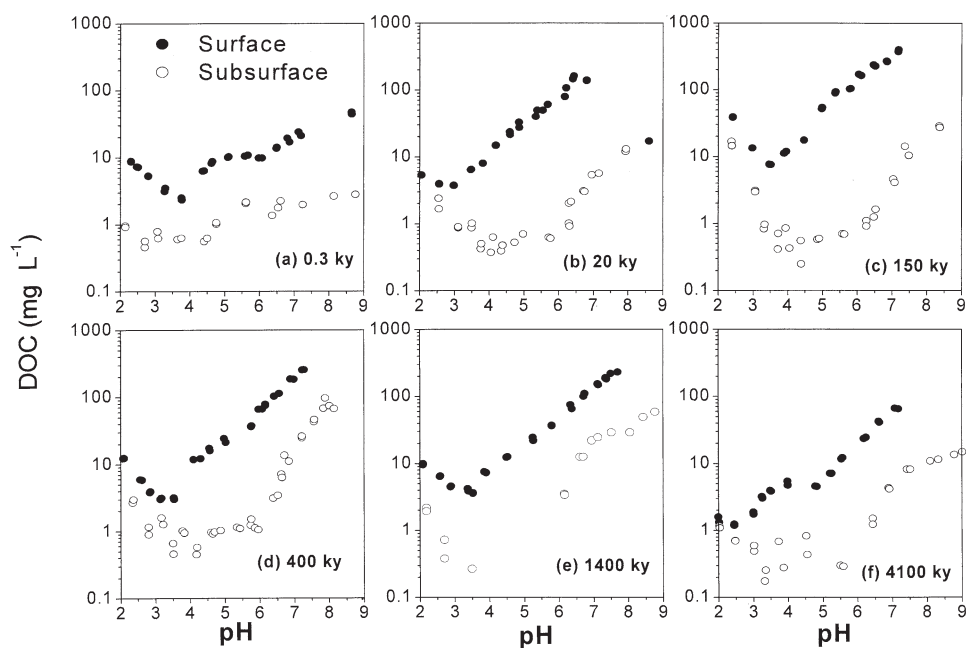


Fig. 9. Dissolution of organic C into LiCl supernatant solutions during discontinuous titration experiments. Data are shown for $I = 10$ mM LiCl, which extends across the widest equilibrium pH range.

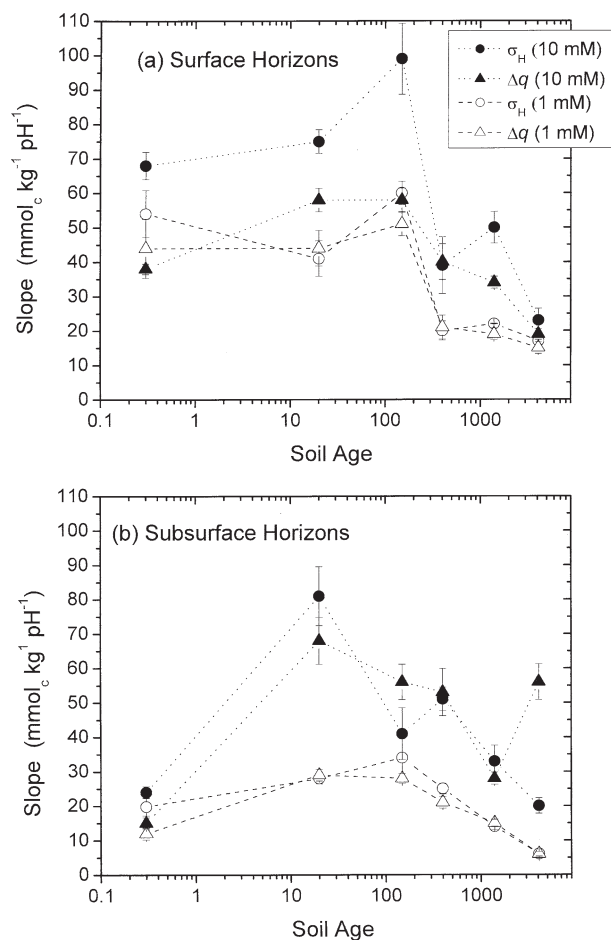


Fig. 10. The magnitude of variable surface charge as measured from linear regression of proton adsorption (circles) or background ion adsorption (triangles) against pH as a function of soil age. Open and filled symbols are for 1 and 10 mM LiCl, respectively. Error bars represent the 95% confidence limits of regression slope.

rise to a wide distribution in surface acid dissociation constants (Stumm, 1992), effectively buffering soil pH over the full range of measurement. Such behavior is expected for complex multicomponent mixtures of hydroxylated mineral and organic constituents (Fig. 2; Table 1) and has been observed in prior studies of variable surface charge in soil systems (Charlet and Sposito, 1987; Chorover and Sposito, 1995a; Skjellberg and Borggaard, 1998).

The σ_H and Δq vs. pH regression slopes ($\delta\sigma_H/\delta\text{pH}$) that provide a measure of the change in surface charge per unit change in pH are plotted as a function of soil age in Figure 10 (error bars represent the 95% confidence interval). In 1.0 mM LiCl, there is no statistical difference ($\alpha = 0.05$) between regression slopes for σ_H and Δq for a given surface (Fig. 10a) or subsurface (Fig. 10b) soil, although surface soils exhibit higher slope than subsurface soils over the LSAG. At higher I (10 mM), the calculated slope for σ_H exceeds that for Δq in the 0.3, 20, 150, and 1400 ky surface soils, and in the 0.3 subsurface soil. In these cases, the slopes for Δq vs. pH are considered a more accurate measure of surface charging. However, for a given soil and I , the difference between slopes for σ_H and Δq

provides a quantitative measure of proton and hydroxide charge consumed during pH dependent DOC release, as discussed in section 4.1. The slope for Δq is only higher in the 4100 ky subsurface soil (Fig. 10b). As a whole, Figure 10 indicates that the intermediate-aged soils exhibit the greatest variable charge density; slopes increase in the surface soils to 150 ky, then decrease with increasing age to 4100 ky (Fig. 10a). The same is true in the subsoil at low I , but at high I , the 20 ky soil exhibits the largest slope.

4.2.3. Role of SOM structure

Time-dependent changes in soil solid chemistry across the LSAG provide an opportunity to evaluate the factors contributing to the high density of variable charge in these soils. Given the large change in mass of SOM in soils across the LSAG (Table 1), its role is certainly paramount. Changes in functional group composition of HAs from A-horizon samples taken across the LSAG are revealed by ^{13}C -NMR spectroscopy (Fig. 3). We focus here on HAs because: (i) they represent a large C fraction of mineral-associated SOM; (ii) they can be

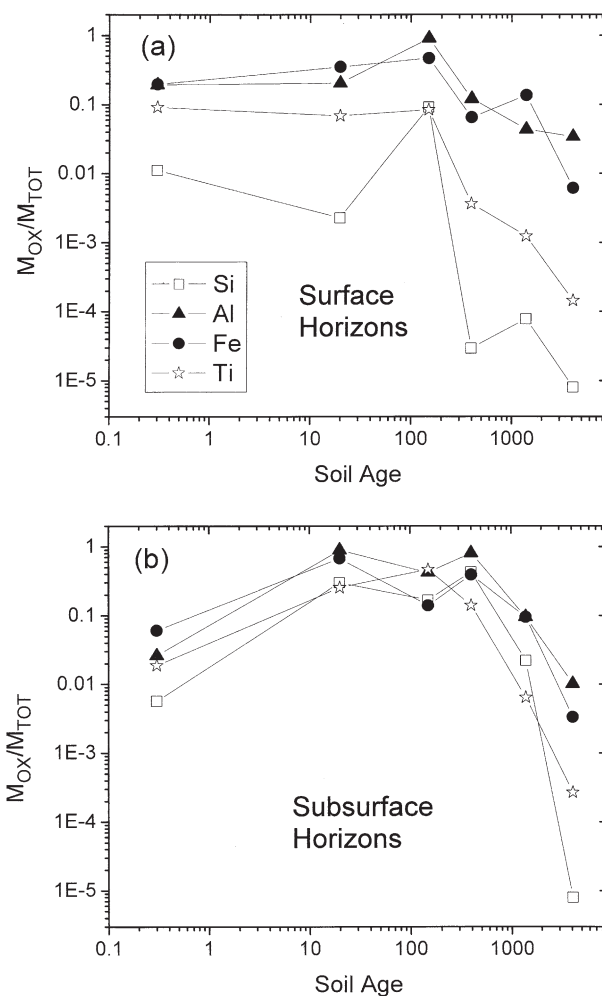


Fig. 11. Mass fractions of total Fe and Al that are extractable in acid oxalate solution (pH 4) for (a) surface soils and (b) subsurface soils, calculated from data presented in Table 2.

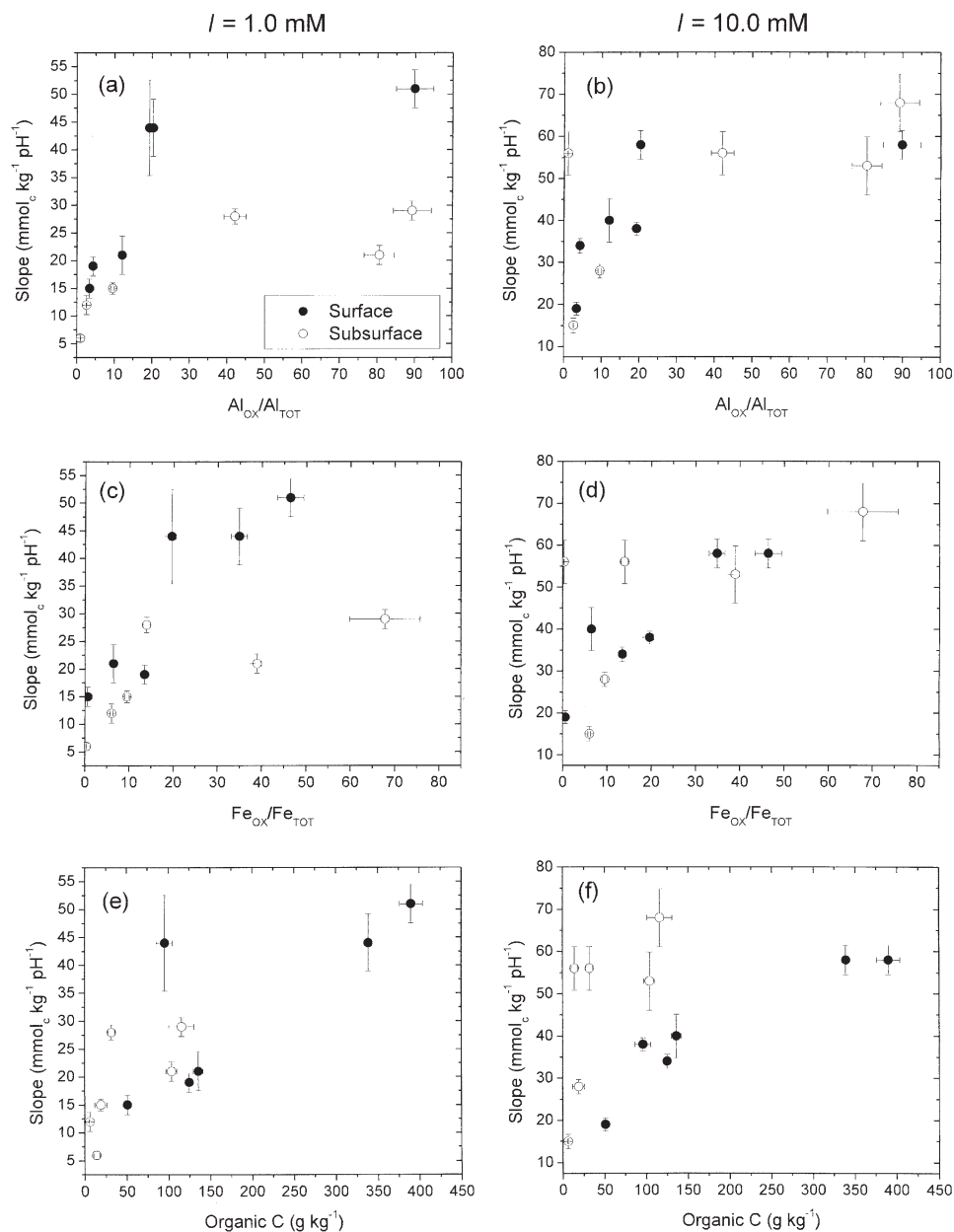


Fig. 12. Scatterplots of surface charging slopes (from Δq vs. pH) against the oxalate extractable fractions of Al and Fe: (a) Al, $I = 1$ mM; (b) Al, $I = 10$ mM; (c) Fe, $I = 1$ mM; and (d) Fe, $I = 10$ mM; and organic C content (e) $I = 1$ mM; (f) $I = 10$ mM.

separated from the soil and purified to remove paramagnetic impurities that complicate NMR data acquisition; and (iii) they exhibit higher charge density relative to humin, the solid phase pool of humic substances that is insoluble in the 0.1 M NaOH extraction (Stevenson, 1994). Relative to the total pool, our analyses indicate an increase in aliphatic (alkyl) C with increasing soil age to 400 ky, apparently at the expense of carbohydrate (O-alkyl) C (Fig. 3b). The greatest difference between the two is at the 400 ky site, where O-alkyl C is lowest and alkyl C is highest, but the ratio of alkyl to O-alkyl C remains high for the oldest soils as well. Relative peak areas for carboxyl and aromatic C show less dramatic change, although an increase in

aromatic C beginning at 400 ky is suggested (Fig. 3b). These results are consistent with a preferential degradation of carbohydrates and an accumulation of more recalcitrant waxes, resins, and lignin degradation products in those soils with the highest SOM (150–400 ky). This observation helps to explain the longer C turnover time in the 150 to 400 ky soils (Torn et al., 1997). Analogous increases in the alkyl/O-alkyl ratio are widely reported to correlate with the extent of organic matter humification (e.g., Norden and Berg, 1990; Baldock et al., 1992; Zech et al., 1992).

Overall, however, the spectra exhibit internal similarity in peak location and shape (Fig. 3a). This consistency of structure

Table 4. Intrinsic acidity constants and points of zero charge of LSAG soils.

Soil Sample	<i>I</i> = 0.001, M					<i>I</i> = 0.001 M				
	pKa ₁ (int) ¹	pKa ₂ (int) ²	PZNPC ³	PZNPC ⁴	PZNC ⁵	pKa ₁ (int)	pKa ₂ (int)	PZNPC ³	PZNPC ⁴	PZNC ⁵
Surface										
(10–20 cm)										
Ola'a A	— ⁶	5.9 (0.2)	5.5 (0.4)	4.6 (0.5)	4.5 (0.3)*	2.2 (0.3)	4.31 (0.08)	4.2 (0.4)	3.5 (0.1)	2.0 (0.2)*
Laupahoehoe A	2.88 (0.07)	5.8 (0.1)	4.4 (0.3)	4.5 (0.3)	2.8 (0.2)*	2.5 (0.3)	4.76 (0.09)	3.4 (0.4)	3.4 (0.2)	1.8 (0.3)*
Kohala A	3.6 (0.17)	5.5 (0.1)	4.9 (0.2)	4.9 (0.2)	3.4 (0.2)*	3.0 (0.3)	5.77 (0.07)	4.4 (0.3)	4.3 (0.4)	1.9 (0.2)*
Pololu A	6.0 (0.23)	—	6.7 (0.4)	6.4 (0.2)	—	4.6 (0.2)	6.67 (0.06)	5.1 (0.3)	5.2 (0.3)	0.9 (0.5)*
Kolekole A	2.5 (0.24)	6.18 (0.07)	4.4 (0.3)	4.5 (0.1)	1.8 (0.4)*	2.9 (0.5)	5.4 (0.22)	4.3 (0.2)	3.3 (0.2)	2.1 (0.2)
Kokee A	—	5.0 (0.1)	3.4 (0.2)	3.4 (0.1)	—	—	3.6 (0.18)	2.7 (0.5)	2.0 (0.1)	1.2 (0.4)*
Subsurface										
(50–70 cm)										
Ola'a B	—	5.4 (0.3)	6.4 (0.4)	4.02 (0.1)	3.1 (0.3)*	—	2.7 (0.49)	3.9 (0.3)	2.1 (0.1)	1.4 (0.3)*
Laupahoehoe B	4.84 (0.04)	—	6.1 (0.3)	6.2 (0.1)	5.4 (0.1)	3.2 (0.4)	6.0 (0.28)	4.3 (0.5)	4.2 (0.4)	3.8 (0.2)
Kohala B	4.3 (0.1)	—	6.8 (0.2)	6.15 (0.1)	3.7 (0.1)	4.4 (0.2)	7.5 (0.14)	6.8 (0.4)	5.6 (0.3)	3.8 (0.2)
Pololu B	5.73 (0.08)	—	6.2 (0.4)	6.2 (0.1)	4.7 (0.2)	4.7 (0.3)	7.4 (0.20)	6.1 (0.1)	5.8 (0.4)	5.3 (0.1)
Kolekole B	3.0 (0.17)	6.57 (0.08)	4.6 (0.2)	4.5 (0.1)	1.3 (0.4)*	—	4.0 (0.32)	2.4 (0.3)	2.4 (0.2)	1.9 (0.2)*
Kokee B	3.8 (0.14)	7.9 (0.17)	5.2 (0.2)	5.24 (0.1)	4.3 (0.2)	—	3.8 (0.21)	2.0 (0.4)	2.5 (0.2)	4.6 (0.2)

¹ pKa₁(int) is -log of the intrinsic equilibrium constant for the surface dissociation reaction: $\equiv\text{SOH}_2^+ = \equiv\text{SOH} + \text{H}^+ (\text{aq})$.

² pKa₂(int) is -log of the intrinsic equilibrium constant for the surface dissociation reaction: $\equiv\text{SOH} = \equiv\text{SO}^- + \text{H}^+ (\text{aq})$.

³ Calculated from proton titration data (Eq. 7).

⁴ Calculated from ion adsorption data (Eq. 8).

⁵ Calculated from ion adsorption data (Eq. 3).

* = extrapolation of quadratic (best-fit) function to pH values lower than the range covered experimentally (see Fig. 5–6).

⁶ Not in the pH range encountered in the experiment.

likely reflects the equalizing impacts of a consistent source of fixed C from *M. polymorpha* (the dominant net primary producer at all LSAG sites) and the metabolic activities of the resident heterotrophic microbiota subjected to constant climate across the LSAG. Despite the evident variability with soil age, as a group, the LSAG HAs exhibit a range in functional group content (Fig. 3b) that is narrower than those for soils sampled from a wider range of forest environments (Hatcher et al., 1981a; Hatcher et al., 1981b; Malcolm, 1989; Kögel-Knabner et al., 1991; Baldock and Preston, 1995). Given the constancy in source of C inputs across the gradient, we conclude that changes in HA structure as revealed by ¹³C-NMR are driven by the evolving mineralogy of the inorganic fraction, and its changing capacity for stabilization of SOM.

4.2.4. Role of poorly crystalline minerals

PC minerals and their complexes with SOM contain a very high density of H⁺-reactive functional groups per unit particle mass (Sposito, 1989) and hence, they are expected to contribute disproportionately (i.e., relative to their mass fraction) to pH dependent charge behavior of the mixture (Parfitt, 1981; Su et al., 1992; Shoji et al., 1993). Although precise quantification of mineral constituents for the LSAG soils is elusive, an *operational* measure is conventionally asserted to be the mass fraction of (hydr)oxide forming metals (M) extracted from the solid phase by reaction with oxalate at pH 4 ($M_{\text{OX}}/M_{\text{TOT}}$) (Jackson et al., 1986). The effects of oxalate reaction on DRIFT spectra (Fig. 2) support this assertion for the LSAG soils (also see section 3.2). Values of $M_{\text{OX}}/M_{\text{TOT}}$ (calculated from the data in Table 2) for Al, Fe, Si, and Ti (Fig. 11) follow trends in soil age and depth which are strikingly similar to those observed for the slopes of surface charging curves (Fig. 10), providing strong

support for the role of PC constituents in conferring the larger magnitude of variable charge on the intermediate-aged soils. Furthermore, hydroxides of Fe and Al appear to be preferentially removed (i.e., exhibit the most rapid dissolution kinetics) in the oxalate extraction, particularly in the surface soils, suggesting enrichment of Fe and Al in the PC fraction.

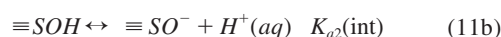
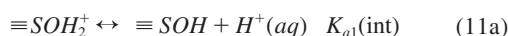
Linear slopes of the charging curves for Δq against pH were plotted against the mass fractions of oxalate extractable to total Al ($\text{Al}_{\text{OX}}/\text{Al}_{\text{TOT}}$) and Fe ($\text{Fe}_{\text{OX}}/\text{Fe}_{\text{TOT}}$), and organic C content (Fig. 12). While there is clearly covariance among these parameters for the LSAG (Tables 1 and 2), their positive relationship with the magnitude of surface charging is likewise apparent (Fig. 12). As a result of covariance and the complex architecture of the soil fabric, it is not possible—nor is it appropriate—to identify a single soil component as the principal driver for enhancement of variable charge. Rather, the data highlight the intense surface reactivity of hydroxide-humic complexes that form in early-to-intermediate stages of pedogenesis in the LSAG soils.

4.3. Points of Zero Charge Indicate Changing Surfaces in Mineral-Organic Complexes

As a result of the preponderance of acidic carboxyl and phenolic OH groups, SOM exhibits a low point of zero net proton charge (PZNPC), typically less than three, and strongly acidic carboxylic groups remain dissociated at pH 2 (Perdue and Lytle, 1983; Tombacz and Meleg, 1990). Therefore, SOM coatings are expected to decrease the PZNPC values of Fe and Al (hydr)oxides, which are typically in the range of six to nine (Stumm, 1992). This surface charge “masking” effect has been observed in prior studies of natural estuarine particles (Hunter and Liss, 1982), kaolinitic tropical soils (Chorover and Sposito,

1995b), and upon adsorption of organic matter to specimen kaolinite (Chorover et al., 1999b) and crystalline Fe and Al (hydr)oxide surfaces (Davis, 1982; Gibbs, 1983). Therefore, evaluation of soil PZNPC values should help to delineate the nature of reactive surface sites for mineral-organic complexes across the LSAG.

Points of zero charge (PZNC and PZNPC) for all soils and ionic strengths are presented in Table 4. The PZNC values are significantly lower than those of PZNPC, as required by charge balance on soil particles comprising negative permanent charge density (Chorover and Sposito, 1995a). Values for PZNPC determined by both proton titration (Eqn. 8) and ion adsorption (Eqn. 9) are compared, since proton titration results have been affected in some cases by H^+/OH^- consumption during SOM dissolution. Microscopic surface acidity constants (pK_{a1} and pK_{a2}) were calculated (Sigg and Stumm, 1981; Stumm, 1992) from the pH dependence of σ_H as determined from the ion adsorption data [$\sigma_H = -(\Delta q + \sigma_0)$]. These are average *intrinsic* (corrected for electrostatic effects) proton dissociation constants that are determined by considering the soil as comprising a simple set of equivalent hydroxylated sites that can undergo proton adsorption and desorption according to the acid-base reactions:



Though simplified representations of a more complex soil surface chemistry (Goldberg, 1992), these constants are presented here to illustrate the relative surface acidities of the different soils and to facilitate synoptic comparison to specimen mineral systems (e.g., Dzombak and Morel, 1990).

The proton surface charge data show an increase in PZNPC and $pK_{a1}(int)$ values with increasing soil age to the intermediate aged sites, followed by a decrease to the oldest sites. Values of PZNPC (determined from ion adsorption data) are depicted graphically in Figure 13. The trending of these data are comparable to that shown for slopes of the surface charging curves (Fig. 10) and the "PC fractions" of Fe and Al (Fig. 11), highlighting the key role of reactive Fe and Al hydroxides in controlling the surface chemistry of the intermediate-aged soils.

It is important to note that, despite the very high organic C contents of the intermediate-aged soils (Table 1), the PZNPC values of these soils more closely approximate those of the resident Fe and Al minerals such as ferrihydrite, Al-rich allophane, and gibbsite (Stumm, 1992; Harsh et al., 2002) than SOM. Thus, we propose a different model for mineral-organic interactions in these soils than one of organic coatings on mineral surfaces. The trends depicted in Figure 13 are more consistent with a scenario where strongly acidic functional groups of macromolecular SOM are increasingly saturated with Fe and Al species and small, high-surface area colloids during early and intermediate stages of pedogenesis (Fig. 14). As a result, the surface chemistry of SOM is masked by coatings of complexed Al, Fe, and their colloidal products, which are so prevalent at this stage of soil development. The relative importance of colloidal hydroxides vs. metal complexes in modulating SOM charge depends on location in the soil profile. The $q_{Al,max}$ near pH 3.5 in surface soils (Fig. 4) suggests that

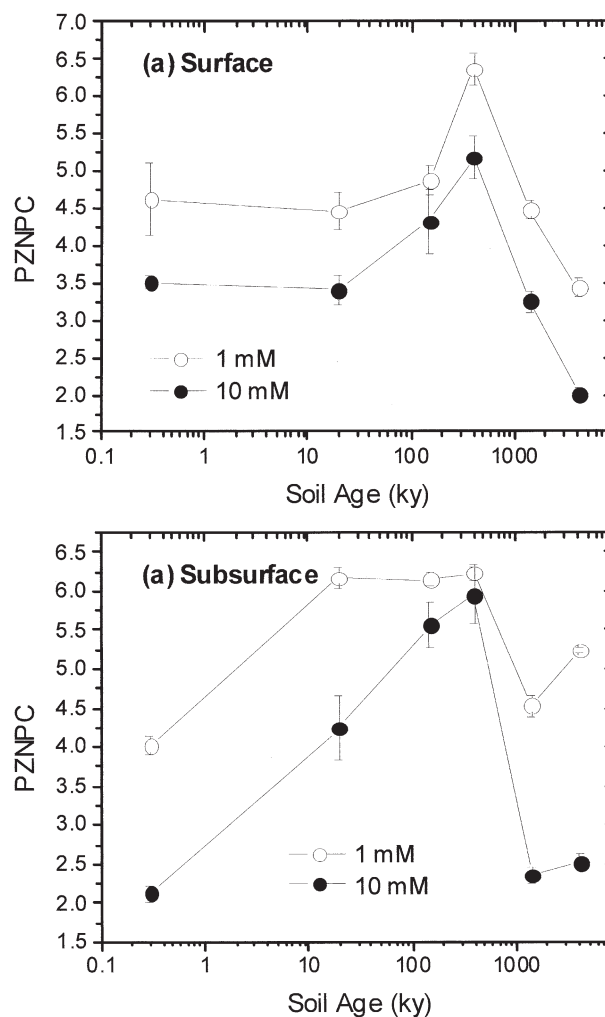


Fig. 13. Point of zero net proton charge (PZNPC) as a function of soil age and I as determined from background ion adsorption data.

competition with H^+ for adsorption sites (Eqn. 7b) on SOM becomes particularly important at high $[H^+]$. Indeed, carboxyl groups of SOM are reported to exhibit a distribution of pK_a values centered near 3.5 to 4 (Perdue and Lytle, 1983). The lower values for q_{Al} in the subsurface, and the absence of a clear maximum, are both consistent with the lower organic C contents of the subsoils (Table 1), which implies a decrease in high-Al-affinity SOM adsorbent. The fact that q_{Al} is diminished in the subsoil (Fig. 4) suggests a greater role at depth for weakly acidic surfaces of hydrous Fe and Al oxides relative to SOM adsorbed Al.

With increasing soil age beyond 150 or 400 ky, PC ferrihydrite, allophane, and goethite are converted to larger, more thermodynamically stable crystals of goethite, kaolinite/halloysite, and gibbsite, whose surface chemistry is increasingly masked by adsorbed coatings of SOM with lower PZNPC (Fig. 14). In respect to mineralogy, structural charge (σ_0) and organic C content, the oldest (1,400 and 4100 ky) LSAG soils are comparable to the highly weathered kaolinitic Oxisols derived from alluvial Andean sediments in isohyperthermic regions of the Brazilian Amazon basin studied by Chorover and

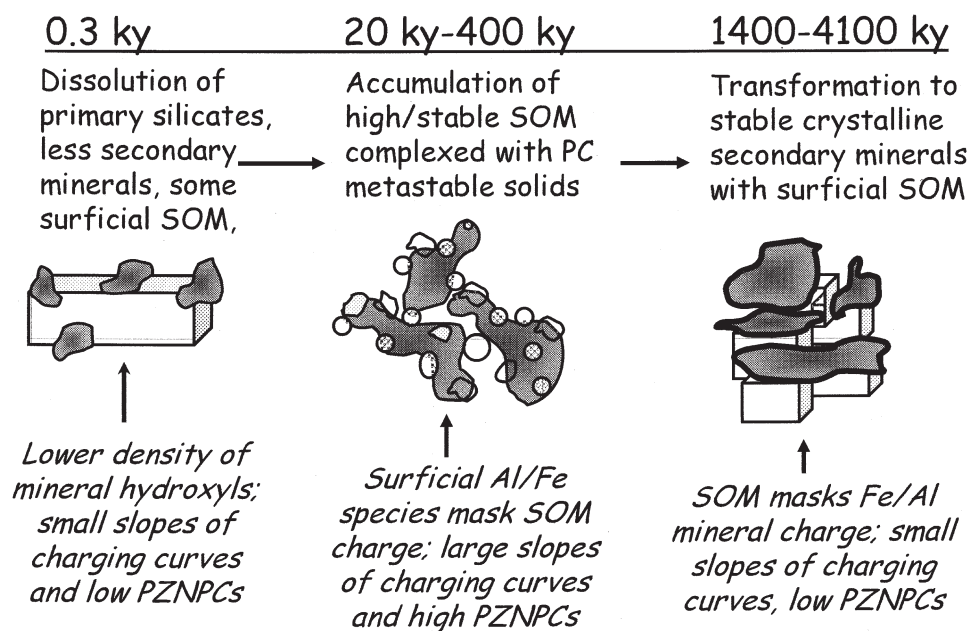


Fig. 14. Proposed changing nature of mineral-organic complexes and effects on surface charge in LSAG soils.

Sposito (1995a). The PZNPC values for the Brazilian soils (calculated from ion adsorption data) ranged from 3.4 to 6.0 in 1 mM LiCl and from 3.4 to 4.8 in 10 mM LiCl. Thus, values for the oldest LSAG soils fall into the range observed for the Brazilian soils at low I and are slightly higher at high I (Table 4). Linearized slopes of charging curves for the Brazilian Oxisols are comparable in magnitude ($5\text{--}20 \text{ mmol}_c \text{ kg}^{-1} \text{ pH}^{-1}$) to those of the oldest LSAG soils, as are the PZNC values, which were consistently lower than corresponding PZNPC values (except for the 4100 ky subsurface soil at 10 mM LiCl), as expected for soils containing small quantities of negative structural charge. Moreover, electrophoretic mobility measurements of clay particles from the Brazilian Oxisols (also comprising dominantly kaolinite, goethite, and gibbsite) revealed a narrow distribution of particle surface charge that was more consistent with that of the SOM coatings than with the underlying heterogeneous mineral assemblage (Chorover and Sposito, 1995b). The convergence of surface charge properties at late weathering stages for these humid-tropical soils from Hawaii and Brazil shows that weathering environment and time can eventually overcome diverse parent lithologies in the course of producing a "climax" mineralogy and surface chemistry.

The pedogenic evolution of mineral-organic complexes may provide some insight into SOM sequestration mechanisms in soils derived from volcanic debris. In a radiocarbon study of the same LSAG chronosequence, Torn et al. (1997) reported a correlation between soil C turnover time and the mineral mass extractable in oxalic acid, both of which were highest in the 150 ky soil (the 400 ky soil was not analyzed in that study). The data presented here suggests that the observed enhancement of SOM stabilization in the intermediate-aged soils is due to the formation of SOM-hydroxy Al and Fe complexes whose surface chemistry is dominated by the metal (hydr)oxide constituents. Saturation of SOM functional groups with monomeric

and polymeric metal hydroxides likely promotes SOM coagulation (Weng et al., 2002; Pranzas et al., 2003), diminishes its bioavailability (Korth et al., 2002) and therefore, increases its long-term recalcitrance in soil. With increased weathering time, transformation from metastable solids to crystalline minerals confers a reduction in Al and Fe species reactivity, which results in a diminished capacity for SOM stabilization, a reduction in C storage, and a shorter turnover time. The proposed pedogenic evolution of mineral-organic complexes across the LSAG is summarized in Figure 14.

5. CONCLUSIONS

The use of proton titration to accurately measure surface charge properties of soils comprising PC mineral-organic complexes requires accounting for proton-consuming side (e.g., dissolution) reactions that do not contribute to charge development. Background ion adsorption was found to provide a more accurate measure of proton surface charge density, based on charge balance, under conditions where significant SOM dissolution occurs, provided that an independent measure of structural charge density is made.

The evolution of surface charge properties in basalt derived soils under humid-tropical climate shows a strong dependence on concurrent changes in soil mineralogy and mineral-associated SOM. In particular, we saw largest values of $\delta\sigma_H/\delta\text{pH}$ in intermediate stage (150–400 ky), and the surface chemistry of Fe and Al (hydr)oxides is increasingly expressed between early and intermediate weathering stages (up to 400 ky in the LSAG) when PC solids (ferrihydrite, allophane, microcrystalline gibbsite) are most prevalent. The fact that organic matter contents are also highest at this stage of pedogenesis suggests that the charge properties of SOM are masked by strong complexation with monomeric and polymeric Fe and Al species (including colloidal hydroxides), and that these species strongly

govern surface charge. Despite enrichment of Fe and Al (relative to Si) in the oldest soils and the predominance of crystalline solids (goethite, crystalline gibbsite, kaolin), the charge properties of the particles in advanced weathering stages appear to be effectively masked by adsorbed organic matter, both in surface soils and at depth. Since the mass fraction of SOM is higher in the intermediate-aged soils than in the oldest soils, the precise nature of mineral-organic associations, rather than the relative abundance of each, appears to exert control on soil surface chemistry.

Acknowledgments—We are grateful to Peter Vitousek for his leadership on the Hawaii Ecosystems Project, to Heraldo Farrington for exceptional management of field logistics and assistance in sampling, and to Patrick Hatcher for use of his NMR spectrometer. We also thank three anonymous reviewers and Associate Editor Nagy for constructive comments on an earlier version of this manuscript. Funding for this work was provided by USDA Program 25.0 in Soils and Soil Biology (# 97–35107–4360).

Associate editor: K. Nagy

REFERENCES

- Aiken G. R., McKnight D. M., and Wershaw R. L. (1985) *Humic Substances in Soil, Sediments and Water*. John Wiley and Sons.
- Anderson S. J. and Sposito G. (1991) Cesium adsorption method for measuring accessible structural charge. *Soil Sci. Soc. Am. J.* **55**, 1569–1576.
- Baes A. U. and Bloom P. R. (1989) Diffuse reflectance Fourier transform infrared (DRIFT) spectroscopy of humic and fulvic acids. *Soil Sci. Soc. Am. J.* **53**, 695–700.
- Baldock J. A. and Preston C. (1995) Chemistry of carbon decomposition processes in forests as revealed by solid-state carbon-13 nuclear magnetic resonance. In *Carbon Forms and Functions in Forest Soils* (ed. W. W. McFee and J. M. Kelly), pp. 89–117, Soil Science Society of America.
- Baldock J. A., Oades J. M., Vassallo A. M., and Wilson M. A. (1992) Aspects of the chemical structure of soil organic materials as revealed by solid-state ¹³C NMR spectroscopy. *Biogeochem.* **16**, 1–42.
- Beckett R. and Le N. P. (1990) The role of organic matter and ionic composition in determining the surface charge of suspended particles in natural waters. *Colloids Surf.* **44**, 35–49.
- Bethke C. M. (2001) *The Geochemist's Workbench*®, Release 4.0, University of Illinois.
- Chadwick O. A. and Chorover J. (2001) The chemistry of pedogenic thresholds. *Geoderma* **100**, 321–353.
- Chadwick O. A., Gavenda R. T., Kelly E. T., Ziegler K., Olson C. G., Elliott W. C., and Hendricks D. M. (2003) The impact of climate on the biogeochemical functioning of volcanic soils. *Chem. Geol.* **202**, 195–223.
- Charlet L. and Sposito G. (1987) Monovalent ion adsorption by an Oxisol. *Soil Sci. Soc. Am. J.* **51**, 1155–1160.
- Chorover J. (2002) Andisols. In *Encyclopedia of Soil Science* (ed. R. Lal), pp. 64–67, Marcel Dekker, Inc.
- Chorover J. and Sposito G. (1995a) Surface charge characteristics of kaolinitic tropical soils. *Geochim. Cosmochim. Acta* **59**, 875–884.
- Chorover J. and Sposito G. (1995b) Colloid chemistry of kaolinitic tropical soils. *Soil Sci. Soc. Am. J.* **59**, 1558–1564.
- Chorover J., DiChiaro M. J., and Chadwick O. A. (1999a) Structural charge and cesium retention in a chronosequence of tephritic soils. *Soil Sci. Soc. Am. J.* **63**, 169–177.
- Chorover J., Amistadi M. K., Burgos W. D., and Hatcher P. G. (1999b) Quinoline sorption on kaolinite-humic acid complexes. *Soil Sci. Soc. Am. J.* **63**, 850–857.
- Cornell R. M. and Schwertmann U. (1996) *The Iron Oxides: Structure, Properties, Reactions, Occurrence and Uses*. VCH Publishers.
- Crews T. E., Kitayama K., Fownes J. H., Riley J. H., Herbert D. A., Mueller-Dombois D., and Vitousek P. M. (1995) Changes in soil phosphorus fractions and ecosystem dynamics across a long chronosequence in Hawaii. *Ecology* **76**, 1407–1424.
- Davis J. A. (1982) Adsorption of natural dissolved organic matter at the oxide/water interface. *Geochim. Cosmochim. Acta* **46**, 2381–2393.
- Delany J. M. and Lundeen S. R. (1989) The LLNL thermochemical database. Lawrence Livermore National Laboratory Report UCRL-21658.
- DiChiaro M. J. (1998) Mineralogy and cesium exchange in a chronosequence of Hawaiian soils derived from volcanic debris. M.S. Thesis in Soil Science, The Pennsylvania State University.
- Dymond J., Biscate P. E., and Rex R. W. (1974) Eolian origin of mica in Hawaiian soils. *Geol. Soc. Am. Bull.* **85**, 37–40.
- Dzombak D. A. and Morel F. M. M. (1990) *Surface Complexation Modeling: Hydrous Ferric Oxide*. John Wiley and Sons.
- Farmer V. C. (1974) The layer silicates. In *The Infrared Spectra of Minerals* (ed. V. C. Farmer), pp. 331–363. Mineralogical Society.
- Gibbs R. J. (1983) Effect of natural organic coatings on the coagulation of particles. *Environ. Sci. Technol.* **17**, 237–240.
- Gislason S. R. and Arnórsson S. (1993) Dissolution of primary basaltic minerals in natural waters: saturation state and kinetics. *Chem. Geol.* **105**, 117–135.
- Gislason S. R., Arnórsson S., and Armannsson H. (1996) Chemical weathering of basalt in SW Iceland: effects of runoff, age of rocks and vegetative/glacial cover. *Am. J. Sci.* **296**, 837–907.
- Goldberg S. (1992) Use of surface complexation models in soil chemical systems. *Adv. Agron.* **47**, 233–329.
- Harsh J., Chorover J. and Nizeyimana E. (2002) Allophane and Imogolite. In *Soil Mineralogy with Environmental Applications* (ed. J. Dixon and D. Schulze), pp. 291–321, Soil Science Society of America.
- Hatcher P. G., Maciel G. E., and Dennis L. W. (1981a) Aliphatic structure of humic acids: a clue to their origin. *Org. Geochem.* **3**, 43–48.
- Hatcher P. G., Schnitzer M., Dennis L. W., and Maciel G. W. (1981b) Aromaticity of humic substances in soils. *Soil Sci. Soc. Am. J.* **45**, 1089–1094.
- Hossner L. R. (1996) Dissolution for total elemental analysis. In *Methods of Soil Analysis: Part 3-Chemical Methods* (ed. D. L. Sparks), pp. 49–64, Soil Science Society of America.
- Hotchkiss S., Vitousek P. M., Chadwick O. A., and Price J. (2000) Climate cycles, geomorphological history and the interpretation of soil and ecosystem development. *Ecosystems* **3**, 522–533.
- Hsu P. H. (1989) Aluminum hydroxides and oxyhydroxides. In *Minerals in Soil Environments* (ed. J. B. Dixon and S. B. Weed), pp. 331–378, Soil Science Society of America.
- Huang P. M. and Schnitzer M. (1986) *Interactions of Soil Minerals with Natural Organics and Microbes*. SSSA Special Publication 17, Soil Science Society of America.
- Hunter K. A. and Liss P. A. (1982) Organic matter and the surface charge of suspended particles in estuarine waters. *Limnol. Oceanogr.* **27**, 322–335.
- Jackson M. L., Levelt T. W. M., Syers J. K., Rex R. W., Clayton R. N., Sherman G. D., and Uehara G. (1971) Geomorphological relationships of tropospherically derived quartz in the soils of the Hawaiian islands. *Soil Sci. Soc. Am. Proc.* **35**, 515–525.
- Jackson M. L., Lim C. H. and Zelazny L. W. (1986) Oxides, hydroxides and aluminosilicates. In *Methods of Soil Analysis: Part 1-Physical and Mineralogical Methods* (ed. A. Klute), pp. 101–150, Soil Science Society of America.
- Jenny H. (1941) *Factors of Soil Formation*. McGraw-Hill Book Company, Inc.
- Jones M. N. and Bryan N. D. (1998) Colloidal properties of humic substances. *Adv. Colloid Interface Sci.* **78**, 1–48.
- Kögel-Knabner I., Hatcher P. G., and Zech W. (1991) Chemical structural studies of forest soil humic acids: aromatic carbon fraction. *Soil Sci. Soc. Am. J.* **55**, 241–247.
- Korth A., Bendinger B., Czekalla C., and Wichmann K. (2002) Biodegradation of NOM in rapid sand filters for removing iron and manganese. *Acta Hydrochim. Hydrobiol.* **29**, 289–297.
- Kurtz A. C., Derry L. A., and Chadwick O. A. (2001) Accretion of Asian dust to Hawaiian soils: isotopic, elemental and mineral mass balances. *Geochim. Cosmochim. Acta* **65**, 1971–1983.
- Lowe D. J. (1986) Controls on the rates of weathering and clay mineral genesis in airfall tephra: a review and New Zealand case study. In

- Rates of Chemical Weathering of Rocks and Minerals* (ed. S. M. Colman and D. P. Dethier), pp. 256–230, Academic Press.
- Malcolm R. L. (1989) Application of solid-state ^{13}C NMR spectroscopy to geochemical studies of humic substances. In *Humic Substances, Volume 2, In Search of Structure* (ed. M. H. B. Hayes et al.), pp 339–371. Wiley Interscience, Chichester, England.
- Morel F. M. M. and Hering J. (1993) *Principles and Applications of Aquatic Chemistry*. Wiley-Interscience.
- Neff J. C., Hobbie S. E., and Vitousek P. M. (2000) Nutrient and mineralogic control on dissolved organic C, N and P fluxes and stoichiometry in Hawaiian soils. *Biogeochem.* **51**, 283–302.
- Norden B. and Berg B. (1990) A non-destructive method (solid-state ^{13}C NMR for determining organic chemical components of decomposing litter. *Soil Biol. Biochem.* **22**, 271–275.
- Parfitt R. L. (1981) Chemical properties of variable charge soils. In *Soils with Variable Charge* (ed. B. K. G. Theng), pp. 167–194, New Zealand Society of Soil Science, Lower Hutt, N.Z.
- Perdue E. M. and Lytle C. R. (1983) Distribution model for binding of protons and metal ions by humic substances. *Environ. Sci. Technol.* **17**, 654–660.
- Pranzas P. K., Willumeit R., Gehrke R., Thieme J., and Knochel A. (2003) Characterisation of structure and aggregation processes of aquatic humic substances using small-angle scattering and X-ray microscopy. *Anal. Bioanal. Chem.* **376**, 618–625.
- Preston C. (1996) Applications of NMR to soil organic matter analysis: history and prospects. *Soil Sci.* **161**, 144–166.
- Preston C. and Blackwell B. A. (1985) Carbon-13 nuclear magnetic resonance for a humic and a fulvic acid: signal to noise optimization, quantitation and spin-echo techniques. *Soil Sci.* **139**, 88–96.
- Russell J. D. and Fraser A. R. (1994) Infrared methods. In *Clay Mineralogy: Spectroscopic and Chemical Determinative Methods* (ed. M. J. Wilson), pp 9–67, Chapman and Hall.
- Shoji S., Yamada I., and Kurashima K. (1981) Mobilities and related factors of chemical elements in the topsoils of andosols in Tohoku, Japan. 2. Chemical and mineralogical compositions of size fractions and factors influencing the mobilities of major chemical elements *Soil Sci.* **132**, 330–346.
- Shoji S., Nanzyo M., and Dahlgren R. A. (1993) *Volcanic Ash Soils: Genesis, Properties and Utilization*. Elsevier Science.
- Sigg L. and Stumm W. (1981) The interaction of anions and weak acids with the hydrous goethite ($\alpha\text{-FeOOH}$) surface. *Colloids Surf.* **2**, 101–117.
- Skjemstad J. O. (1992) Genesis of podzols on coastal dunes in southern Queensland. 3. The role of aluminum-organic complexes in profile development *Austr. J. Soil Res.* **30**, 645–665.
- Skyllberg U. and Borggaard O. K. (1998) Proton surface charge determination in Spodosol horizons with organically bound aluminum. *Geochim. Cosmochim. Acta* **62**, 1677–1689.
- Sposito G. (1989) *The Chemistry of Soils*. Oxford University Press.
- Sposito G. (1998) On points of zero charge. *Environ. Sci. Technol.* **32**, 2815–2819.
- Stevenson F. J. (1994) *Humus Chemistry, 2nd Edition*. John Wiley and Sons.
- Stumm W. (1992) *Chemistry of the Solid-Water Interface*. John Wiley and Sons.
- Su C., Harsh J. B., and Bertsch P. M. (1992) Sodium and chloride adsorption by imogolite and allophanes. *Clays Clay Miner.* **40**, 280–286.
- Swift R. S. (1996) Organic matter characterization. In *Methods of Soil Analysis: Part 3-Chemical Methods* (ed. D. L. Sparks), pp. 1011–1069, Soil Science Society of America.
- Tombacz E. and Meleg E. (1990) A theoretical explanation of the aggregation of humic substances as a function of pH and electrolyte concentration. *Org. Geochem.* **15**, 375–382.
- Torn M. S., Trumbore S. E., Chadwick O. A., Vitousek P. M., and Hendricks D. M. (1997) Mineral control of soil organic carbon storage and turnover. *Nature* **389**, 170–173.
- Vitousek P. M. (2004) *Nutrient Cycling and Limitation: Hawaii as a Model System*. Princeton University Press.
- Vitousek P. M., Chadwick O. A., Crews T. E., Fownes J. H., Hendricks D. M., and Herbert D. (1997) Soil and ecosystem development across the Hawaiian islands. *GSA Today* **7**, 1–8.
- Wada K. (1995) Role of aluminum and iron in the accumulation of organic matter in soils with variable charge. In *Environmental Impact of Soil Component Interactions* (ed. P. M. Huang), pp. 47–58, CRC Press.
- Wada K. and Aomine S. (1973) Soil development on volcanic materials during the Quaternary. *Soil Sci.* **116**, 170–177.
- Weng L., Temminghoff E. J. M., and van Riemsdijk W. H. (2002) Interpretation of humic acid coagulation and soluble soil organic matter using a calculated electrostatic potential. *Eur. J. Soil Sci.* **53**, 575–587.
- Whittig L. D. and Allardice W. R. (1986) X-ray diffraction techniques. In *Methods of Soil Analysis: Part 1-Physical and Mineralogical Methods* (ed. A. Klute), pp. 331–362, Soil Science Society of America.
- Zech W., Ziegler F., Kögel-Knabner I., and Haumaier L. (1992) Humic substances distribution and transformation in forest soils. *Sci. Tot. Environ.* **117/118**, 155–174.